ORIGINAL ARTICLE

Plant, Cell & Environment PCE **WILEY**

High-throughput field phenotyping reveals genetic variation in photosynthetic traits in durum wheat under drought

Nícolas Zendonadi dos Santos[1] | Hans-Peter Piepho[2] | Giuseppe Emanuele Condorelli[3] | Eder Licieri Groli[3] | Maria Newcomb[4] | Richard Ward[4] | Roberto Tuberosa[3] | Marco Maccaferri[3] | Fabio Fiorani[1] | Uwe Rascher[1] | Onno Muller[1]

[1]Institute of Bio- and Geosciences, IBG-2: Plant Sciences, Forschungszentrum Jülich GmbH, Jülich, Germany

[2]Biostatistics Unit, Institute of Crop Science, University of Hohenheim, Stuttgart, Germany

[3]Department of Agricultural and Food Sciences, University of Bologna, Bologna, Italy

[4]Maricopa Agricultural Center, University of Arizona, Maricopa, Arizona, USA

Correspondence
Nícolas Zendonadi dos Santos and Onno Muller, Institute of Bio- and Geosciences, IBG-2: Plant Sciences, Forschungszentrum Jülich GmbH, 52428 Jülich, Germany.
Email: n.zendonadi@fz-juelich.de and o.muller@fz-juelich.de

Abstract

Chlorophyll fluorescence (ChlF) is a powerful non-invasive technique for probing photosynthesis. Although proposed as a method for drought tolerance screening, ChlF has not yet been fully adopted in physiological breeding, mainly due to limitations in high-throughput field phenotyping capabilities. The light-induced fluorescence transient (LIFT) sensor has recently been shown to reliably provide active ChlF data for rapid and remote characterisation of plant photosynthetic performance. We used the LIFT sensor to quantify photosynthesis traits across time in a large panel of durum wheat genotypes subjected to a progressive drought in replicated field trials over two growing seasons. The photosynthetic performance was measured at the canopy level by means of the operating efficiency of Photosystem II (F_q'/F_m') and the kinetics of electron transport measured by reoxidation rates (F_{r1}' and F_{r2}'). Short- and long-term changes in ChlF traits were found in response to soil water availability and due to interactions with weather fluctuations. In mild drought, F_q'/F_m' and F_{r2}' were little affected, while F_{r1}' was consistently accelerated in water-limited compared to well-watered plants, increasingly so with rising vapour pressure deficit. This high-throughput approach allowed assessment of the native genetic diversity in ChlF traits while considering the diurnal dynamics of photosynthesis.

KEYWORDS
chlorophyll fluorescence, electron transport, fluctuating environment, genetic diversity, photosynthesis, physiological breeding, spatiotemporal modelling

1 | INTRODUCTION

Light energy absorbed by chlorophylls can (a) drive photosynthesis (photochemistry), (b) be thermally dissipated or (c) be re-emitted as light (fluorescence), and these three processes coexist in competition (see details in Baker, 2008; Maxwell & Johnson, 2000; Stirbet, Lazár, Guo, & Govindjee, 2020). Chlorophyll *a* fluorescence emanates from both Photosystem (PS) II and PSI, and at room temperature, it is mainly emitted by PSII at wavelengths between 650–780 nm, peaking at around 685–740 nm (Drusch et al., 2017). There has been a long-standing acknowledgment that ChlF-derived parameters are powerful, inexpensive, fast and non-invasive tools for probing photosynthesis

and, therefore, for monitoring the physiological status of plants, even remotely (Baker, 2008; Drusch et al., 2017; Govindjee, 2004; Kalaji et al., 2017; Krause & Weis, 1984, 1991; Mohammed et al., 2019; Murchie & Lawson, 2013). The operating light use efficiency of PSII (F'_q/F'_m), for instance, has been demonstrated to be a reliable parameter to monitor the linear electron transport (LET) from water through PSII and PSI, and consequently, provides a good relative measure of the quantum yield of CO_2 assimilation (ϕ_{CO_2}) in both C_3 and C_4 plants, when photorespiration is at a minimum (Genty, Briantais, & Baker, 1989; Habash, Paul, Parry, Keys, & Lawlor, 1995; Krall & Edwards, 1990). Biotic and abiotic stresses disturb this linear relationship due to concurrent electron-driven biological processes apart from CO_2 assimilation (Baker, 2008). However, even in harsh conditions, ChlF has proven to be a robust integrative technique for assessing plant photosynthetic performance (Baker & Rosenqvist, 2004; Kalaji et al., 2017; Pérez-Bueno, Pineda, & Barón, 2019; Wang et al., 2018).

Owing to its retrievable optical signal, ChlF is detectable and quantifiable by passive-based instruments (e.g., spectrophotometers), depending solely on solar irradiance (i.e., sun-induced fluorescence, SIF), or by active-based instruments (e.g., fluorometers), using artificial excitation light sources (Aasen et al., 2019; Cendrero-Mateo et al., 2016; Mohammed et al., 2019). Due to technological advances, chlorophyll fluorometry techniques have rapidly evolved, and commercial instruments for measuring ChlF in plants have become available. In the last decades, several studies have taken advantage of this approach to assess the impact of water deficit on an extensive list of plant species, ranging from native Mediterranean plants (e.g., rosemary and lavender) to various agricultural crops, including barley, wheat, rice, maize, beans, soybean, cotton, potato and grapevine (Kao & Tsai, 1998; Longenberger, Smith, Duke, & McMichael, 2009; Mathobo, Marais, & Steyn, 2017; Nogués & Alegre, 2002; O'Neill, Shanahan, & Schepers, 2006; Oukarroum, Madidi, Schansker, & Strasser, 2007; Ranalli, di Candilo, & Bagatta, 1997; Wada, Takagi, Miyake, Makino, & Suzuki, 2019; Wang et al., 2012; Yan et al., 2017; Zivcak, Kalaji, Shao, Olsovska, & Brestic, 2014). By far, the vast majority of the prior research has relied on the pulse-amplitude modulation (PAM) fluorometry (Schreiber, 1986). This commonly used technique typically requires a dark-adaptation and/or a saturating flash in very close proximity, mostly done by clamping on leaves. However, such requirements can be time-consuming, have limited application at a distance and are prohibitive in less accessible field locations (Cendrero-Mateo et al., 2017; Osmond et al., 2017). Hence, despite the advantages of using ChlF for monitoring plant physiological status, applying this method to a large number of experimental units growing in open fields, as is required for plant breeding programmes, is still challenging.

Attempts to exploit new molecular tools to their full potential, particularly to dissect the genetics of quantitative traits, such as yield and stress tolerance, are limited by our ability to quantify relevant traits with the necessary throughput (Araus & Cairns, 2014; Tuberosa, 2012). Integration of high-throughput phenotyping with genotyping may lead to a major breakthrough in our understanding of the fundamentals of complex adaptive physiological traits related to drought tolerance (Edmeades, McMaster, White, & Campos, 2004;

Reynolds et al., 2020; van Eeuwijk et al., 2019). High-throughput phenotyping platforms (HTPPs) have been deployed to quantify ChlF and other traits to circumvent existing bottlenecks in phenotypic and genomic selection (e.g., Barbagallo, Oxborough, Pallett, & Baker, 2003; Chen et al., 2014; Flood et al., 2016; Humplík et al., 2015; Jansen et al., 2009; McAusland, Atkinson, Lawson, & Murchie, 2019; Tschiersch, Junker, Meyer, & Altmann, 2017; Wang et al., 2018). However, they are generally confined to operate under controlled or semi-controlled environments and restricted to detached leaves or small and medium-sized plants, and only a few are suitable for large plants (>1.50 m). HTPPs for measuring ChlF under natural fluctuating field conditions (e.g., the "Field Scanalyzer" reported by Virlet, Sabermanesh, Sadeghi-Tehran, & Hawkesford, 2017) are hitherto scarce.

More recently, the LIFT fluorometer (Kolber et al., 2005) has emerged as an alternative high-throughput approach for continuous remote measurement of the photosynthetic status of terrestrial vegetation (Ananyev et al., 2005). The LIFT method monitors ChlF induction and relaxation within milliseconds using subsaturating excitation flashlets in a fast repetition rate (FRR) instead of the saturating pulse (Kolber, Prášil, & Falkowski, 1998). This pump-and-probe technique works at a distance, bridging the gap between leaf and canopy levels and has demonstrated a great potential for monitoring agricultural systems (Pieruschka, Klimov, Kolber, & Berry, 2010; Raesch, Muller, Pieruschka, & Rascher, 2014; Rascher & Pieruschka, 2008; Wyber, Osmond, Ashcroft, Malenovský, & Robinson, 2018). LIFT-measured ChlF empirically provides not only PAM-analogous photosynthetic parameters but also measures the downstream electron transport rates (ETR) from the primary quinone acceptor (Q_A) to the plastoquinone (PQ) pool, and ultimately, towards PSI (Osmond et al., 2017; Osmond, Chow, Pogson, & Robinson, 2019; Pieruschka et al., 2010). By monitoring the kinetics of LIFT-based ETR over different timeframes beyond Q_A, Keller, Vass, et al. (2019) developed the Q_A^- reoxidation efficiency parameters ($F'_{r1;r2}$) for photosynthesis phenotyping. Using the LIFT method for automated plant phenotyping under semi-field conditions, Keller, Matsubara, et al. (2019) demonstrated that the ChlF-based parameters not only facilitated the understanding of photosynthetic interactions with varying environmental factors but also identified differences between and within crop species. Nevertheless, to the best of our knowledge, the LIFT approach has not yet been applied to large-scale field phenotyping of ChlF traits under natural fluctuating growing conditions.

Here, we aimed to assess the inherent genetic variation in photosynthetic traits at the canopy level in a large durum wheat panel (>220 elite accessions) under progressive drought in the field. The photosynthetic performance was measured using the LIFT method by means of ChlF traits: F'_q/F'_m and the newly developed reoxidation efficiency parameters, F'_{r1} and F'_{r2}, which were slightly modified from Keller, Vass, et al. (2019). In particular, our study aimed (a) to estimate relevant population parameters (genotypic variation and heritability) for the LIFT-measured ChlF traits; (b) to evaluate the phenotypic plasticity of ChlF-related traits in response to drought; (c) to assess correlations between ChlF traits and relative change in leaf relative water content (ΔRWC), or total shoot dry matter yield (SDMY); and (d) to

assess the effects of a fluctuating environment, in terms of light intensity and vapour pressure deficit (VPD), and their interactions with varying soil moisture, on ChlF traits.

2 | MATERIALS AND METHODS

2.1 | Plant material

In two growing seasons, we evaluated a set of elite durum wheat (*Triticum turgidum* L. ssp. d*urum* Desf.) accessions, mainly cultivars and advanced lines, from the association mapping population "UNIBO-Durum Panel" assembled at the University of Bologna (UNIBO), Italy (see list of materials in Table S1). This panel contains a representative selection of the genetic diversity existing in the major improved durum wheat gene pools adapted to Mediterranean environments (Maccaferri et al., 2006, 2011). The collection includes "founder genotypes" used extensively worldwide as parents in breeding programmes, as well as accessions bred and released by CIMMYT (the International Maize and Wheat Improvement Centre), ICARDA (the International Centre for Agricultural Research in the Dry Areas), INRAE (the French National Institute for Agriculture, Food and Environment), IRTA (the Spanish Institute of Agriculture and Food Research and Technology) and by public breeding programmes in Italy, in the Northern Great Plains of the USA and Canada (North Dakota, Montana, Saskatchewan and Alberta), and materials from the Southwestern USA, namely "Desert Durum®", which are co-owned by the Arizona Grain Research and Promotion Council and the California Wheat Commission. Recently, Condorelli et al. (2018) reported the occurrence of a strong population genetic structure in the UNIBO-Durum Panel, identifying eight distinct subpopulations, despite a considerable admixture mostly among germplasm from ICARDA, CIMMYT and Italy. These subgroups were also considered for further assessment in our study.

2.2 | Experimental design

Field experiments were conducted at the Maricopa Agricultural Centre of the University of Arizona (33.07454°N, 111.97494°W, elevation 360 m) in Maricopa, AZ, on a Casa Grande sandy loam soil (fine-loamy, mixed, superactive, hyperthermic Typic Natrargids) under a semi-arid low desert climate. In the first growing season 2017/2018 (Year 1 = Y1), a total of 252 accessions were planted on November 28, 2017, while in the subsequent season, 2018/2019 (Year 2 = Y2), 224 accessions were planted on December 18, 2018. In both trials, genotypes were sown in 2-row plots, 3.5 m long with 0.76 m between rows, with an average seeding rate of 16.8 seeds per meter, which were laid out in a resolvable row-column design (Patterson & Williams, 1976; Piepho, Williams, & Michel, 2015) with two replicates (14 rows × 18 columns per rep) in Y1, and with three replicates (14 rows × 16 columns per rep) in Y2. Pre-plant granular nitrogen fertilizer at 112 kg/ha and phosphorus (P_2O_5) at 56 kg/ha was incorporated into the soil. Fields were managed following the standard agricultural practices for the region and were regularly monitored to prevent damage from above-ground insect pests and pathogens.

Sprinkler irrigation was used to germinate seeds and establish the crop, followed by subsurface drip irrigation as needed for optimal plant growth, once or twice a week. The pressurized subsurface drip irrigation system was installed before planting when one dripline with emitters spaced every 0.30 m was buried at ~0.10 m depth along each seed row. In Y1, the final irrigation event was on March 11, 2018 (i.e., 103 days after sowing, DAS) when ~50% of the genotypes had flag leaf sheaths opened (i.e., at growth stage [GS] 47; Zadoks et al., 1974). From this time point, the whole experiment was subjected to a progressive water deficit until 2–3 April 2018 when plants at the anthesis halfway stage (GS65, on average) were harvested to measure total above-ground biomass. By contrast, in Y2, on March 5, 2019 (77 DAS), when ~50% of the genotypes were at late tillering phase (GS26), well-watered (WW) and water-limited (WD) treatments were implemented and assigned to entire single seed rows in an alternating pattern across the field, such that the initial 2-row plots where split into two side by side subplots of one row each (i.e., a strip-plot type design with water treatment as one main-plot factor). Due to operational limitations, the water treatment could not be randomized, and this alternating pattern of WW and WD strips was assigned to keep a homogeneous field. Control subrows remained well watered by recurring subsurface drip irrigation, whereas water-stressed subrows experienced a progressive water deficit. Both water treatments were imposed until April 9, 2019 (112 DAS) at early anthesis (GS61, on average) when the experiment was terminated, and plots were harvested to determine total above-ground biomass. Table S2 summarizes both growing seasons.

2.3 | Meteorological data and soil moisture monitoring

Daily and hourly meteorological reports for both growing seasons were obtained from the Arizona Meteorological Network (AZMET; https://cals.arizona.edu/azmet/06.htm). In addition, high temporal resolution meteorological data, particularly air temperature, relative humidity and photosynthetic photon flux density (PPFD), for the experimental site were recorded at 5-second intervals with an automated weather station (Clima Sensor US, Adolf Thies GmbH & Co. KG, Göttingen, Germany) and a quantum sensor (SQ-214, Apogee Instruments, Inc., Logan, UT, USA). These data were made available by the TERRA Phenotyping Reference Platform (TERRA-REF; https://terraref.org/). VPD was calculated as the difference between the saturation and actual vapour pressure (Allen, Pereira, Raes, & Smith, 1998).

In Y1, the soil volumetric water content (VWC) was monitored in and between seed rows with time-domain reflectometry (TDR) sensors (True TDR-315, Acclima, Inc., Meridian, ID, USA) installed at three locations within the experiment and at 1 cm, 10 cm and 50 cm depths at each location. In Y2, the TDR sensors (True TDR-310S, Acclima, Inc., Meridian, ID, USA) were installed in both WW and WD seed

rows at three locations within the experimental field at 2, 10, 25 and 50 cm depths and at 15 and 35 cm depths between seed rows. Additional soil sensors were installed between rows at 15 cm depth for measuring the soil matric potential (Tensiomark, ecoTech GmbH, Bonn, Germany). All soil sensors recorded data at 15-min intervals throughout the entire growing seasons. Based on characterisations of the soil hydraulic and physical properties of the experimental site by Prof. Dr Markus Tuller at the University of Arizona (Tucson, AZ) under the TERRA-REF project, the permanent wilting point (θ_{PWP}) and the field capacity (θ_{FC}) at 10–15 cm depth, based on the van Genuchten (1980) model, corresponded to approximately 0.110 and 0.282 m^3/m^3, respectively.

2.4 | Leaf relative water content

The plant water status was monitored by leaf relative water content (RWC) as described by Mullan and Pietragalla (2012). In Y1, flag leaf samples from all plots (252 genotypes × 2 reps) were collected on March 12, 2018 (104 DAS) to measure the initial RWC (iRWC), and on March 27, 2018 (119 DAS) to measure the final RWC (fRWC). The relative change in RWC [%Δ] was calculated at the plot level as $\left[\Delta RWC = \frac{fRWC - iRWC}{iRWC} \times 100\right]$. In Y2, young fully expanded leaves from all plots of a single replicate (224 genotypes × 2 water treatments) were sampled on March 26, 2019 (98 DAS and 21 days after imposing the irrigation treatments). Excised leaf samples were inserted into plastic tubes, sealed, placed in a cooled and insulated container, and immediately transferred to the laboratory. Fresh samples were weighted (FW) and then submerged in distilled water for 12 hr at 4°C in the dark. After rehydration, samples were quickly blotted dry with a paper towel, and the turgid weight (TW) was recorded. After oven-drying for 3 days at 60°C, total dry weight (DW) was recorded. Leaf RWC [%] was then determined as the ratio $\left[RWC = \frac{FW - DW}{TW - DW} \times 100\right]$ (Barrs & Weatherley, 1962).

2.5 | Plant height and above-ground biomass

Plant height was manually measured with a metre stick as the distance from the soil surface to the spike's base or the uppermost level of leaves in the absence of the spike. Median height was measured in the central portion of the plots to reduce plot edge effects. In Y1, plant height was recorded only once at 122 DAS, whilst multiple measurements over time (82, 93, 101 and 107 DAS) were taken in Y2.

Plants were harvested before the ripening stage (Table S2), and therefore biomass data indicate the status at a point in time rather than direct estimates of final yields. In Y1, at the end of the experiment (125–126 DAS), plants within the 2-row plots were cut with a mechanical forage harvester (Carter Manufacturing Company, Inc.) for above-ground whole plot weights, while subsamples for moisture content [%] were hand-cut before mechanical harvesting for measurements of fresh weight and dry weight after oven-drying for 2–3 days. Total shoot dry matter yield (SDMY) was adjusted to 0% moisture and is reported as

(kg/ha). In Y2, the experiment was ended at 112 DAS, and SDMY was obtained for two replicates by hand-cutting lengths of 0.914 m of plants from each single-row plot (WW and WD), which were bundled and placed into large driers until a constant weight was achieved.

2.6 | LIFT device and method

Active ChlF was measured by means of a portable LIFT instrument (model LIFT-REM 1.0, Soliense Inc., Shoreham, NY, USA; https://soliense.com/LIFT_Terrestrial.php), which induces and records the resulting changes in the ChlF yield of a target leaf/plant canopy at a distance of up to 5 m. The LIFT apparatus relies on the FRR fluorescence technique (Kolber et al., 1998), using high-frequency subsaturating excitation pulses, or "flashlets", of a blue (λ 445 nm) light-emitting diode (LED) to manipulate the level of photosynthetic activity of PSII. A 685 nm ± 10 nm optical interference filter separates the red ChlF emission from the reflected excitation light. The system operates with the FRR fluorescence saturation/relaxation protocol with variable duty cycles. Firstly, during the saturation phase (SQ_A), at a high duty cycle, the Q_A in PSII reduces progressively, leading to a transient increase in ChlF yield. Subsequently, during the relaxation phase (RQ_A), at an exponentially decreasing duty cycle, Q_A reoxidizes, as electrons flow towards PSI, and the ChlF yield decreases (Kolber et al., 2005; Osmond et al., 2017).

In our study, the Q_A flash reproduced the $FRRF_{0.75ms}$ protocol introduced by Keller, Vass, et al. (2019). According to this protocol, the SQ_A phase (lasting ~0.75 ms) consists of a sequence of 300 subsaturating flashlets (1.6 μs pulse length) applied at 2.5 μs discrete intervals. The RQ_A phase (lasting ~209 ms) consists of 127 flashlets (1.6 μs pulse length) with an initial interval between flashlets of 20 μs followed by exponential increments. The exponent factor increases from 1.025 to 1.05, linearly over the RQ_A sequence's length to best cover the temporal dynamics of the fluorescence relaxation signal. At a distance of 0.60 m, the average excitation power for the SQ_A phase was ~72,000 μmol photons m^{-2} s^{-1} in Y1 and ~55,000 μmol photons m^{-2} s^{-1} in Y2. Excitation power was measured at a 1% duty cycle using a 5-second calibration flash (a sequence of 50,000 flashlets with 1 μs pulse length at 100 μs intervals) measured by a quantum sensor (LI-190R, LI-COR, Inc., Lincoln, NE).

Apart from the ChlF sensor, the LIFT device is also equipped with a Vis micro-spectrometer (STS-VIS, Ocean Optics, Inc., Winter Park, FL) with an optical resolution of 1.5 nm (FWHM) for acquiring spectral bands between 400–800 nm (integration time 790 ms). Acquisition of spectral data was synchronized to be performed immediately after completion of each LIFT Q_A flash.

2.7 | Field measurements

The LIFT instrument was installed to the front end of a cart (model based on White & Conley, 2013) in the vertical direction pointing downward (nadir) and above the plant canopy, perpendicular to the

crop row (Figure S1). The distance from the LIFT lens to the median uppermost-canopy (i.e., the target area) was ~0.60 m, being regularly adjusted as plants grew. The blue LED light beam was ~30 mm in diameter at the focal point over the target area. The fluorescence channel's gain was adjusted at the beginning of each measurement day to maintain the raw fluorescence within the 2,000–20,000 signal range, aiming to operate with an optimal signal-to-noise ratio.

Regardless of the growing season, the day of measurement and the time of day, the cart's front end was always facing south to avoid self-shadowing over the target area. The cart was manually pushed across the plots at an average speed of 8 cm/s while a total of 20 independent measurements, each one carried out in a time frame of ~1 s, were acquired from every experimental unit per day of measurement. In Y1, the entire field trial (252 genotypes × 2 reps) was measured at 0, 1, 2, 3, 4, 5, 6, 8, 10, 12 and 16 days after withholding water (DAWW). On average, measurements were performed between 09:20–16:40 hours local Mountain Standard Time (MST). In Y2, aiming to achieve three different levels of drought severity between WW and WD (D1, D2 and D3), field data were collected at three time points after imposing water treatment. However, due to the size of the trial (224 genotypes × 2 treatments × 3 replicates), only one replicate per day was operationally possible between 08:45–15:55 hr MST, on average. Thus, three consecutive days were required to phenotype the entire experiment with three replicates: D1 was taken between 12 and 14 days after imposing water treatment, D2 between 17 and 19 days and D3 between 23 and 25 days. Further field operational details related to the LIFT data collection are reported in Figures S2 and S3.

The spectral data were calibrated by a 0.50 m × 0.50 m white reference panel with 95% reflectance (Zenith Lite™ diffuse target, SphereOptics GmbH, Herrsching, Germany) horizontally placed at 0.60 m in front of the LIFT apparatus (Figure S1b). Over a field phenotyping day, white reference measurements were regularly taken every 36 plots (~30-min interval) in Y1 and 32 plots (~25-min interval) in Y2. Dark reference measurements were acquired in a dark room with the LIFT lens covered with a dark cloth.

2.8 | Data processing

2.8.1 | Fluorescence parameters for field phenotyping

Based on a slight modification of the procedure reported by Keller, Vass, et al. (2019), we derived the photosynthetic traits from the LIFT-measured ChlF transients using the Q_A flash protocol. The PSII operating efficiency (F'_q/F'_m) from light-adapted plants was estimated as $\left[\frac{F'_m - F'}{F'_m}\right]$, where F' is the ChlF yield of the first flashlet and F'_m is the maximum ChlF yield observed between flashlets 298th and 302nd inclusive (Figure S4).

The Q_A^- reoxidation efficiency trait (Fr') is typically estimated by integrating the ChlF yield curve at a specific time interval and using the normalized integral area as a proxy for the slope of the ChlF transient to assess the kinetics of the relaxation phase (Keller, Matsubara,

et al., 2019; Keller, Vass, et al., 2019). Here, however, we directly assessed these kinetics by fitting log–log regression models for the time intervals of interest, namely t_1 from 0.82 to 1.44 ms (i.e., from 303rd to 320th flashlets) and t_2 from 1.56 to 8.08 ms (i.e., from 321st to 360th flashlets), where both variables, independent (time) and dependent (ChlF yield), were log-transformed. According to the power-law relationship $f(x) = \alpha x^\beta$, the slope and the constant of a straight line from a log–log model equal β and $\log \alpha$, respectively (Marquet et al., 2005). Therefore, the efficiency of electron transport up to ~0.65 ms after reducing Q_A in light-adapted plants (1) was estimated as the slope β of the log–log regression fitted within the t_1 interval, while the efficiency of electron transport up to ~6.64 ms after $Fr1'$ (i.e., $Fr2$) was equal to the slope β of the log–log model fitted within the t_2 interval (Figure S4). The time intervals t_1 and t_2 approximate the time frame in which electron transfer from Q_A to the PQ pool, and to some extent from the PQ pool to PSI, respectively (de Wijn & van Gorkom, 2001; Govindjee, 2004; Keller, Vass, et al., 2019; Kolber et al., 1998; Osmond et al., 2017, 2019; Stirbet & Govindjee, 2011). These time intervals are also supported by various in silico models (Lazár, 2003; Lazár & Jablonský, 2009; Stirbet & Strasser, 1995; Xin, Yang, & Zhu, 2013; Zhu et al., 2005). Moreover, in our study, the time intervals for estimating t_1 and t_2 remained the same regardless of genotype, water treatment and/or growing season.

The phenotypic plasticity of a given genotype for a ChlF trait in Y1 was based on the overall drought-induced relative change (%Δ), being estimated as $\left[\frac{\text{ChlF}_{final} - \text{ChlF}_{initial}}{\text{ChlF}_{initial}} \times 100\right]$, where $\text{ChlF}_{initial}$ is the mean value of genotype i for a ChlF trait (F'_q/F'_m, $Fr1'$ or F'_{r2}) at 0 DAWW (non-stress), and ChlF_{final} is the mean value of genotype i for a ChlF trait at 16 DAWW (severe stress).

2.8.2 | Spectral reflectance

The calibrated reflectance was estimated by normalising the target spectrum against the dark and white references. Thus, plant canopy reflectance [%] at 1 nm interval from 400 to 800 nm was calculated as $\left[\frac{\text{DN}_{raw} - \text{DN}_{dark}}{\text{DN}_{white} - \text{DN}_{dark}}\right]$, where DN_{raw} is the raw digital value of the target, DN_{dark} is the dark reference measurement and DN_{white} is the white reflectance measurement (Bruning, Berger, Lewis, Liu, & Garnett, 2020). As red edge-based vegetation indices have been shown as good indicators of leaf area index (LAI), leaf and canopy chlorophyll content and plant water content (Bruning et al., 2020; Dong et al., 2019; Filella & Peñuelas, 1994; le Maire, François, & Dufrêne, 2004; Liu et al., 2004; Liu, Miller, Haboudane, & Pattey, 2004; Mutanga & Skidmore, 2007), we derived the Vogelmann red edge index (VOGREI) from the calibrated spectrum reflectance as the ratio $\left(\frac{\lambda 740\,\text{nm}}{\lambda 720\,\text{nm}}\right)$ (Vogelmann, Rock, & Moss, 1993).

2.8.3 | Data cleaning

We collected a total of 110,880 and 80,640 ChlF transients (and spectral data) over time in Y1 and Y2, respectively. The LIFT sensor relies

on its artificial excitation light source to induce ChlF emission from the target canopy, and a ChlF transient, such as in Figure S4, is only possible in the presence of living photosynthetic tissues. However, due to the highly fluctuating environment, particularly solar irradiation and winds, shifting of the leaves, off-target measurements (e.g., soil), and/or technical constraints, low-quality data can occur. Hence, a data cleaning pipeline was defined and implemented in the R environment (R Core Team, 2020). Further details about the criteria for data cleaning are in Appendix A (see after the reference list). After this step, the remaining data points, 100,947 (91%) and 77,946 (97%) ChlF transients in Y1 and Y2, respectively, were averaged, resulting in one value per trait per plot per time of measurement ($N = 5,544$ data points per trait in Y1; and $N = 4,032$ data points per trait in Y2). The raw data and the processed and cleaned datasets for both growing seasons are publicly accessible (https://doi.org/10.5281/zenodo.4305673).

2.9 | Statistical analysis

A linear mixed model (LMM) approach was used to analyse the resolvable row-column designs with repeated measures for both Y1 and Y2. Single-stage analysis models were applied to partition variance components and to estimate genotypic effects for all traits based on "Best Linear Unbiased Prediction" (BLUP) (Robinson, 1991). Variance components for each trait were estimated by residual maximum likelihood (REML) using the Average Information (AI) algorithm with sparse matrix methods (Gilmour, Thompson, & Cullis, 1995), as implemented in GENSTAT (VSN International, 2019). For random terms, the variance components were set to be positive-constrained. Details regarding the baseline models (BL), with covariates (BL$_{Cov}$) and spatiotemporal modelling (BL$_{Cov+STM}$), as well as the model selection with LMM are in Appendix B (see after the reference list). The adjusted coefficient of determination (R^2_{adj})-like statistic for the final "best" LMM was estimated based on the average semivariance approach (Ω^{ASV}_β), as proposed by Piepho (2019). Conditional F test statistic was used to test fixed effects. The Fisher–Hayter procedure, a modified LSD (MLSD) test using the Studentized Range statistic (Hayter, 1986), was used to perform pairwise comparisons between adjusted means.

The impact of adding covariates and modelling the spatiotemporal correlations was evaluated by means of relative efficiency (RE) in terms of the error size. Thus, RE was used to assess the improvement in precision of the alternative models over the BL models (i.e., models without covariates and/or spatiotemporal covariance structures) for Y1 and Y2, respectively. The RE [%] was calculated as suggested by Qiao, Basford, DeLacy, and Cooper (2000) and can be defined as $\left(\frac{SED_{BL}}{SED_{AT}} \times 100\right)$, where SED is the REML-based average standard error of the difference between genotype means for the baseline model (SED$_{BL}$) and for the alternative models (SED$_{AT}$). The higher the RE estimate, the better the precision of the field evaluation of genotypes.

2.10 | Heritability and trait correlation estimation

Broad-sense heritability on an entry-mean basis (H^2), or repeatability, of a trait for a single time point was estimated according to Cullis, Smith, and Coombes (2006) as

$$H^2 = 1 - \frac{\overline{\nu}^{BLUP}_{\Delta\cdot\cdot}}{2\sigma^2_g},$$

where $\overline{\nu}^{BLUP}_{\Delta\cdot\cdot}$ is the mean variance of a difference of two BLUPs for the genotypic effect and σ^2_g is the genotypic variance.

Bivariate LMM (see details in Piepho, 2018; Piepho & Möhring, 2011) were used to estimate genetic correlations (r_g) between each pair of traits (e.g., between ChlF traits and SDMY or ΔRWC) in each time point. Details regarding these models are in Appendix B. Coefficients of phenotypic correlation r_p between traits over time were estimated by Pearson's coefficients of correlation between the BLUEs ("Best Linear Unbiased Estimators"; Appendix B) of genotypes.

2.11 | Covariates and spatiotemporal modelling

Before covering our key findings, here we report the overall outputs of model selection with LMM. The model fit for the ChlF traits considerably improved after accounting for the biological and experimental sources of variation, as well as for the spatiotemporal correlations among neighbouring plots (Table S3). All models fitted to ChlF traits for Y1 and Y2 are reported in Tables S4–S9, respectively. The addition of fixed regression coefficients on top of the baseline models (i.e., BL$_{Cov}$) to accommodate differences in plant height (i.e., RelF), in plant growth and development (iZDS or ZDS), in canopy structure and leaf pigments (i.e., VOGREI), along with fluctuating environmental factors which were recorded at a 5-s interval (e.g., PPFD and VPD), promoted a net gain in precision, in terms of relative efficiency (RE) estimates, by 25.5, 28.9 and 23.4%, on average, for F'_q/F'_m, F'_{r1} and F'_{r2}, respectively. Models with the further addition of spatiotemporal trends (BL$_{Cov+STM}$) resulted in smaller but meaningful gains in precision relative to BL$_{Cov}$, yielding total final improvements of 29.6, 36.5 and 27.3%, on average, for F'_q/F'_m, F'_{r1} and F'_{r2}, respectively. These final "best" fit models (BL$_{Cov+STM}$, as indicated in Tables S4–S9), whose coefficients of determination (Ω^{ASV}_β) ranged from .49 to .73 (Table S3), served as the basis for all results hereafter reported. The conditional F test statistics for fixed effects are found in Table S10.

3 | RESULTS

3.1 | Weather conditions and drought severity

Overall, south-central Arizona's climate conditions were quite distinct between the two growing seasons. According to the National Centres

for Environmental Information (NOAA, 2020), the 6-month period (November–April) in the 2017/2018 season (Y1) was characterized as the warmest and the driest on record for a 126-year period (1895–2020), whereas the 2018/2019 season (Y2) was the 53rd warmest and the 75th driest for the same period. The average temperature, precipitation and Palmer Z Index, as a measure of short-term drought severity, for the 6-month period (Nov-Apr) in Y1 were 16.6°C (+3.0°C anomaly compared to the 1901–2000 mean), 41.7 mm (−99.1 mm anomaly) and −2.28 (severe drought; −2.39 anomaly), against 13.9°C, 147.3 mm and 0.19 in Y2, overall a near-normal season (NOAA, 2020).

Mean meteorological data for the time period when LIFT data were recorded in both growing seasons are found in Figure S5. The higher atmospheric water demand in Y1 led to a faster and more acute reduction in soil moisture compared to Y2 (Figure S6). After withholding water, θ_{PWP} at 10 cm depth was reached in roughly 3 and 17 days in Y1 and Y2, respectively. From this time point until the last day of field measurements using the LIFT sensor, the soil VWC dropped ~27.1% up to 16 DAWW in Y1, and only ~11.2% up to 25 DAWW in Y2. The WD rows in Y2 were, on average, 31.1% drier at 10 cm depth compared to the WW counterpart rows at D1, even though soil VWC was still slightly above (~8.5%) the θ_{PWP} (Figure S6). At the D2 and D3 time points, WD rows were, on average, 43.1 and 45.5% drier than WW rows, respectively. The soil VWC for WD rows was around and slightly below (~10.0%) the θ_{PWP} in D2 and D3, respectively (Figure S6). Overall, soil moisture in WW rows at 10 cm depth remained at 68.5% (standard deviation, $SD = 7.2$) of the θ_{FC} over time in Y2.

3.2 | Effects of water stress on leaf RWC and above-ground biomass

In Y1, when the drought was severe, the mean relative change in leaf RWC (ΔRWC) from 0 to 15 DAWW was −25.3%Δ (Figure S7a). High variability among the 252 genotypes was observed ($p < .001$), where ΔRWC for the least and the most dehydrated genotypes were −14.9%Δ (standard error, $SE = 1.98$) and −44.1%Δ ($SE = 2.98$), respectively. In Y2, when the drought was milder, even after imposing 21 days of water-limiting conditions, leaf RWC of WD plants decreased, on average, only by −1.83%Δ ($SE = 0.13$) compared to WW plants (Figure S7b). Despite this mild stress and a minor drop in RWC in Y2, the water treatment had a major effect on the total shoot dry matter yield (SDMY), $F(1, 27.2) = 176$, $p < .001$, where WD plants produced, on average, 4,815 kg/ha ($SE = 52.4$), and WW plants produced 6,020 kg/ha ($SE = 65.6$). Although SDMY greatly varied among genotypes ($p < .001$) in Y2, the genotype-by-water treatment interaction was not significant ($p = .258$). In Y1, the mean SDMY at the end of the severe stress was 5,161 kg/ha, varying from 4,343 kg/ha ($SE = 146$) to 5,801 kg/ha ($SE = 267$) among genotypes ($p < .001$; Figure S7a). However, because the progressive drought was imposed throughout the entire experiment, a comparison with a WW condition within the same growing season was not possible.

3.3 | Effects of drought stress on ChlF traits

The increasing severity of drought stress condition in Y1 resulted in a slow but steady reduction in F'_q/F'_m and in both reoxidation efficiency
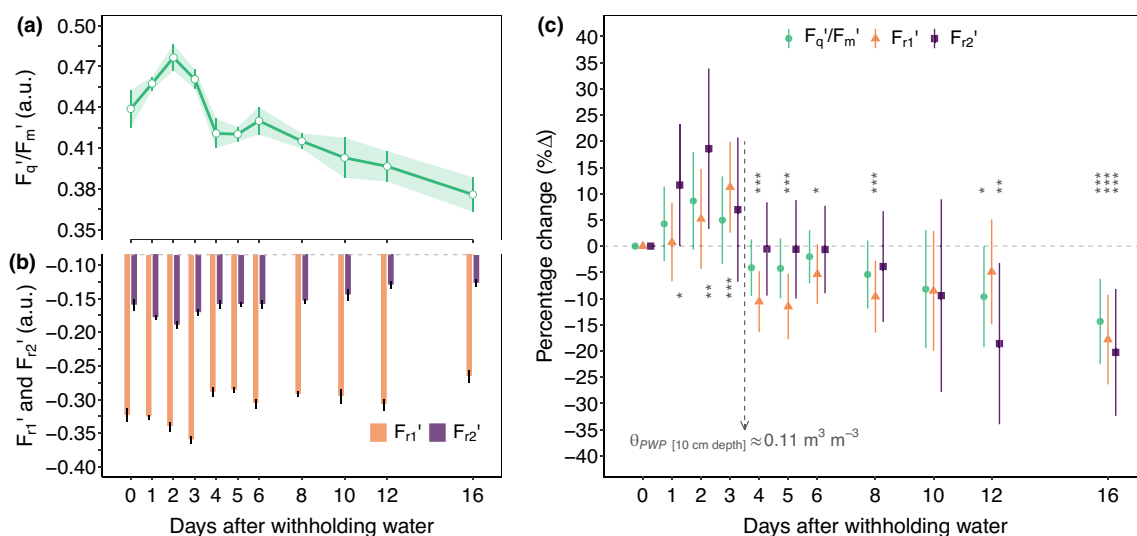

FIGURE 1 LIFT-measured chlorophyll fluorescence (ChlF) traits from light-adapted durum wheat plants in response to progressive drought stress, from 0 to 16 days after withholding water (DAWW), in Y1. (a) Operating efficiency of PSII (F'_q/F'_m); and (b) efficiency of electron transport up to □0.65 ms after reducing Q_A (i.e., F'_{r1}; the kinetics of electron transfer from Q_A to PQ pool), and up to □6.64 ms after F'_{r1} (i.e., F'_{r2}; the kinetics of electron transfer from PQ pool to PSI). Values are means, averaged across genotypes, with ±95% confidence intervals (CIs), $n = 252$. (c) Percentage changes (%Δ) in ChlF traits over time. Mean relative changes with ±95% CIs are shown with respect to the baseline value at 0 DAWW. Pairwise comparisons between time points and baseline within each ChlF trait were performed by the Fisher–Hayter procedure. The levels of significance are indicated by * ($p ≤ .05$), ** ($p ≤ .01$), and *** ($p ≤ .001$), otherwise blank if $p > .05$. Dashed arrow indicates when the soil permanent wilting point ($\theta_{PWP} = 0.11$ m³/m³) at 10 cm depth was reached

traits, F'_{r1} and F'_{r2} (Figure 1a,b). At 16 DAWW, F'_q/F'_m, F'_{r1} and F'_{r2} significantly decreased by −14.4, −17.8 and −20.3%, respectively, relative to 0 DAWW (Figure 1c). This down-regulation of ChlF traits was well aligned with the combined effect of progressive soil moisture dry-down at 10 cm and 50 cm depths (Figure S8). Indeed, the soil VWC at 50 cm depth strongly correlated with overall daily means for ChlF traits (Figure 2). Although linearly slowing down over time, F'_{r1} tended to accelerate immediately after the onset of drought (up to 3 DAWW) before decelerating in the long term (Figures 1c and 2b). Simultaneously, θ_{PWP} at 10 cm depth was reached around 3 DAWW.

The overall main effect of water treatment in Y2, averaged across time, was minor but significant for F'_q/F'_m, $F(1, 13.3) = 54.7$, $p \le .001$, where WD plants (mean, $M = 0.507$, $SE = 0.0008$) had slightly higher values than WW plants ($M = 0.497$, $SE = 0.0008$). In addition, F'_{r1} for WD plants ($M = -0.368$, $SE = 0.001$) was faster than for WW plants ($M = -0.347$, $SE = 0.001$), $F(1, 13.0) = 205$, $p < .001$. However, F'_{r2} for both treatments, WD ($M = -0.212$, $SE = 0.0006$) and WW ($M = -0.210$, $SE = 0.0006$), performed alike, $F(1, 13.4) = 1.73$, $p = .211$. The water treatment-by-time interaction was significant for F'_q/F'_m, $F(2, 111) = 5.99$, $p = .003$ and for F'_{r1}, $F(2, 111) = 29.1$, $p < .001$, but of minor effect for F'_{r2}, $F(2, 110) = 2.01$, $p = .139$. At time point D1, when the soil in the WD rows was only marginally dry, F'_q/F'_m for WD plants was +1.08% relative to control plants (Figure S9). At D2 and D3, with further depletion of soil VWC, stressed plants showed higher F'_q/F'_m compared to non-stressed plants, +2.72% and +2.58%, respectively (Figure S9). Likewise, F'_{r1} for WD plants was faster than for WW plants throughout the season in the order of +3.10%, +7.50% and +7.86% for D1, D2 and D3, respectively (Figure S9). These drought-induced trends for F'_{r1} in Y2 (milder drought) were similar to those observed at the onset of the water-limiting conditions in Y1, particularly around 3 DAWW (Figure 1c).

Independently of the environment, the three ChlF traits operated in a highly coordinated manner, which was observed in Y1 (Figure 3) across multiple time points with varying ambient conditions, either above or below ground. Daily means for F'_{r1} and F'_q/F'_m (Figure 3a) were strongly correlated, indicating that the faster or slower the electron flow from Q_A towards PQ pool, the higher or lower the PSII operating efficiency. Moreover, F'_{r2} and F'_q/F'_m (Figure 3b) were even better correlated, suggesting that the faster or slower the electron flow from PQ pool towards PSI, the higher or lower the PSII operating efficiency. Interestingly, this correlation was even stronger than the relationship between both reoxidation processes, F'_{r1} and F'_{r2} (Figure 3c).

3.4 | Phenotypic plasticity and variability across subpopulations

The relationships between overall drought-induced percentage changes (%Δ), as a measure of phenotypic plasticity and initial (non-stress) or final (severe stress) values for ChlF traits were evaluated for the subgroups of genotypes (Figure 4). For this assessment, we grouped genotypes into subpopulations (S) based on the genetic structure in the UNIBO-Durum Panel reported by Condorelli et al. (2018), as follows: S1 includes Mediterranean and North African germplasm; S2 includes cultivars bred for dryland areas at ICARDA (Syria) in the early 1970s; S3 includes mainly IRTA (Spain) and INRAE (Morocco) accessions bred in early 1970s, and CIMMYT and ICARDA accessions selected for temperate areas; S4 contains predominantly high-yielding materials for temperate zones from ICARDA, and some Italian accessions from the 1970s; S5 comprises materials derived from broadly adapted (photoperiod-insensitive) CIMMYT germplasm released between the late 1970s and the early 1980s; S6 includes Italian accessions from the mid-1970s; S7 includes mostly high-yielding CIMMYT genotypes released from the late 1980s and the early 1990s; S8 contains American (North Dakota), Canadian, French and Australian genotypes; and finally, mostly due to a significant exchange of genetic resources among international breeding programmes, an admixture subgroup is composed mainly by ICARDA, CIMMYT and Italian materials.

A weak negative correlation was found between the initial F'_q/F'_m values for genotypes under well-watered conditions at 0 DAWW and their respective %Δ after experiencing severe drought up to 16 DAWW (Figure 4a). On the other hand, moderate positive correlations were found for F'_{r1} (Figure 4b) and F'_{r2} (Figure 4c), whose initial values explained (by means of R^2) nearly 20 and 45%, respectively, of variability in %Δ throughout genotypes. Nevertheless, there was a strong positive correlation between the final F'_q/F'_m values for genotypes at 16 DAWW and their corresponding overall drought-induced percentage changes (Figure 4d), which explained around 70% of the variability. Similarly, there was a very strong correlation (negative) for final F'_{r1} values (Figure 4e), which explained almost 90% of %Δ variability. Final F'_{r2} values (Figure 4f) were moderately and negatively correlated with their respective %Δ, explaining roughly 30% of the variability. In short, based on Figure 4a,b, it is possible to state that F'_q/F'_m and F'_{r1} from non-stressed plants inform little about the a posteriori effect of drought across genotypes. On the other hand, F'_q/F'_m and F'_{r1} from severely stressed plants can better indicate those genotypes most and least affected by drought (i.e., with the highest and the lowest %Δ), Figure 4d,e. Notably, F'_{r2} from both non-stressed and severely stressed plants may serve as indicators of the potential magnitude of drought effect across genotypes, but interpretations require caution since opposite relationships occurred (Figure 4c,f). It is noteworthy that genotypes grouped at the tail end of %Δ within each ChlF trait (i.e., the two extreme groups of 15 genotypes ranked at the top and bottom according to drought-induced relative changes in F'_q/F'_m, F'_{r1} or F'_{r2}) also had contrasting means for leaf ΔRWC, but equal means for SDMY (Table S11).

The variation among subpopulations alone accounted for approximately 7.5 ($p < .001$), 8.0 ($p < .001$) and 16.7% ($p < .001$) of the overall observed variation in the drought-induced %Δ for F'_q/F'_m, F'_{r1} and F'_{r2}, respectively. The subgroup S8 had the lowest overall %Δ in ChlF traits (Table S12), suggesting that genotypes from S8 were less prone to reduce photosynthetic activities even after severe drought stress.
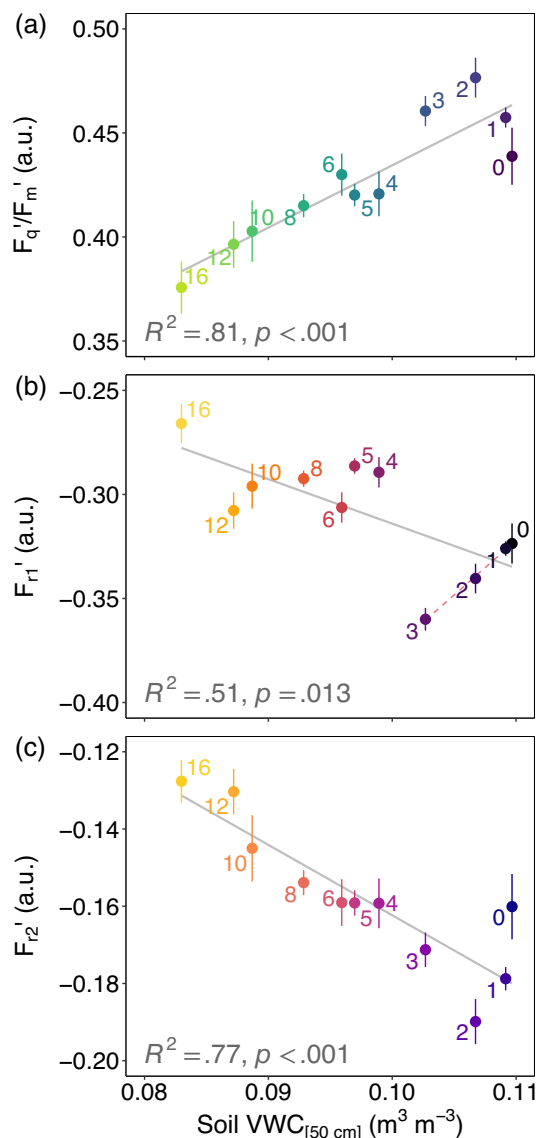
FIGURE 2 Relationships between LIFT-measured chlorophyll fluorescence traits from light-adapted durum wheat plants and the soil volumetric water content (VWC) at 50 cm depth in Y1. (a) Operating efficiency of PSII (F_q'/F_m'); and both reoxidation processes, (b) F_{r1}' and (c) F_{r2}'. Values are means, averaged across genotypes, with ±95% confidence intervals, $n = 252$. Nearby points, the numerical label indicates the timing (in days) after withholding water (DAWW). The colour schemes indicate drought progression over time, from non-stress (darker colours) to severe stress (lighter colours) [Colour figure can be viewed at wileyonlinelibrary.com]

3.5 | Changes of heritability over time

Varying temporal dynamics of genotypic effects were observed for all ChlF traits during progressively increasing drought severity in Y1. The broad-sense heritability (H^2; Figure 5) for F_q'/F_m' increased from 0.55 to 0.64 between 0 to 5 DAWW (i.e., from non-stress to moderate drought) and then gradually decreased to 0.46 in severe drought at 16 DAWW. H^2 for F_{r1}' marginally increased to 0.59 within the first two DAWW, remained stable up to five DAWW, and then

continuously decreased to 0.40 up till 16 DAWW (Figure 5). H^2 for F_{r2}', likewise, had starting values of 0.61, peaked at 0.68 in 3 DAWW and decreased to a minimum of 0.40 (Figure 5). The unknown (residual) environmental effects increased from moderate to severe stress conditions, which could explain the decline in heritabilities (i.e., the decreasing relative contribution of genetic effects to phenotypic variance). The overall BLUP of genotypic values averaged across time for Y1 are reported in Figure S10.

For Y2, on average, H^2 for F_q'/F_m', F_{r1}' and F_{r2}' were 0.65, 0.74 and 0.64, respectively, regardless of time (drought severity) and water treatment (WD and WW). Neither the genotype-by-treatment interaction effect nor the three-way interaction of genotype, treatment and time for ChlF traits were significant ($p > .10$) under the mild drought conditions in Y2. Figure S11 shows the overall BLUP of genotypic values, irrespective of water treatment and time.

Values of H^2 for SDMY and ΔRWC were 0.63 and 0.80, respectively, under the severe drought conditions in Y1. Moreover, H^2 for SDMY was 0.45 for both WD and WW plants in Y2 since the genotype-by-water treatment interaction effect was not significant ($p = 0.26$).

3.6 | Trait–trait genetic and phenotypic correlations

Bivariate LMMs for testing the genetic overlap between traits (see Methods) were fitted to investigate the trait–trait genetic correlations (r_g) over time between ChlF traits and SDMY or ΔRWC. The correlation patterns changed according to the drought severity (Figure 6). The r_g between F_q'/F_m' and SDMY (Figure 6a) decreased during the steady progression of drought, with the highest positive correlation at 1 DAWW (0.65, $SE = 0.14$, $p < .001$), and a weak negative correlation at 16 DAWW (-0.21, $SE = 0.34$, $p = .274$). Both F_{r1}' and F_{r2}' (Figure 6a) showed similar r_g patterns with final SDMY over time, and they mirrored that displayed by F_q'/F_m'. During the mild drought in Y2, the r_g between ChlF traits and final SDMY (Figure S12) were, on average, 0.70, -0.45 and -0.65 for F_q'/F_m', F_{r1}' and F_{r2}', respectively, which were similar to those correlations observed at the onset of water-limiting conditions in Y1, particularly between 1 and 5 DAWW.

Time-varying genetic correlations were also evident between ChlF traits and the relative change in leaf RWC (Figure 6b). Within the first week after withholding water, r_g between F_q'/F_m' and ΔRWC was, on average, -0.36, and increased to 0.35 ($SE = 0.28$, $p = .128$) under severe stress at 16 DAWW. On the other hand, an opposite trend was seen for both reoxidation traits, F_{r1}' and F_{r2}', whose r_g with ΔRWC were, on average, 0.36 and 0.31, respectively, throughout the first week after imposing drought, and then shifted to -0.33 ($SE = 0.22$, $p = .109$) and -0.34 ($SE = 0.33$, $p = .162$), respectively, at 16 DAWW. For these same plants experiencing severe stress in Y1, r_g between SDMY and ΔRWC was -0.43 ($SE = 0.10$, $p < .001$).

Trait–trait phenotypic correlations (r_p) over time between ChlF traits and SDMY (Figure 7a) or ΔRWC (Figure 7b) were estimated by Pearson's correlation coefficients. Similar to the genetic correlations
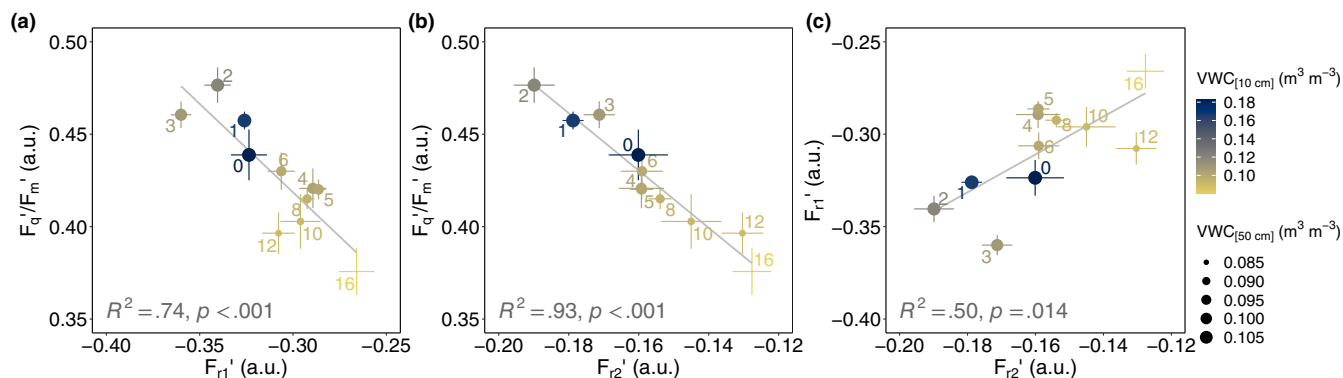
FIGURE 3 Relationships among LIFT-measured chlorophyll fluorescence traits from light-adapted durum wheat plants under progressive drought stress in Y1. (a) Relationship between F'_{r1} (the kinetics of electron transport from Q_A to PQ pool) and operating efficiency of PSII (F'_q/F'_m); (b) relationship between F'_{r2} (the kinetics of electron transport from PQ pool to PSI) and F'_q/F'_m; and (c) relationship between both reoxidation processes, F'_{r1} and F'_{r2}. Values are means, averaged across genotypes, with ±95% confidence intervals, $n = 252$. Nearby points, the numerical label indicates the timing (in days) after withholding water (DAWW). The colour scale for points is based on the soil volumetric water content (VWC) at 10 cm depth, and the point sizes are based on the soil VWC at 50 cm depth [Colour figure can be viewed at wileyonlinelibrary.com]
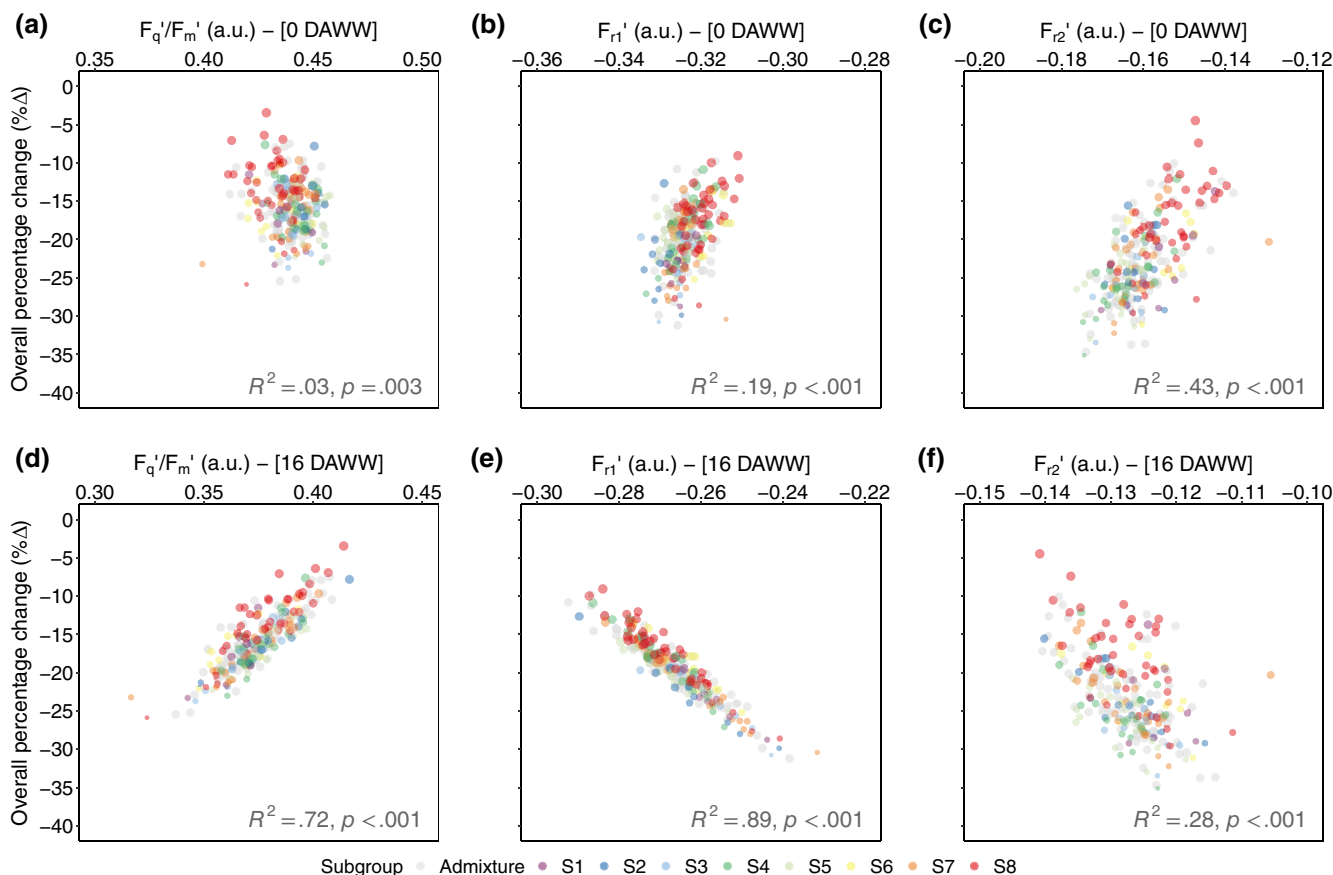

FIGURE 4 Relationships across durum wheat genotypes between the overall drought-induced percentage changes (%Δ; i.e., the size of the absolute change between 0 to 16 DAWW in comparison to the reference value at 0 DAWW) in chlorophyll fluorescence (ChlF) traits and their initial (a) F'_q/F'_m, (b) F'_{r1}, and (c) F'_{r2} values from non-stressed plants at 0 days after withholding water (DAWW), or their final (d) F'_q/F'_m, (e) F'_{r1}, and (f) F'_{r2} values from severely stressed plants at 16 DAWW in Y1. Genotypes were assembled into subgroups (S) according to the population genetic structure reported by Condorelli et al. (2018) [Colour figure can be viewed at wileyonlinelibrary.com]

(Figure 6), the phenotypic correlation patterns dynamically changed according to the drought severity. Indeed, all results for r_p exhibited analogous trends to those described for the trait–trait r_g, but the magnitude of the phenotypic associations was lower, especially between ChlF traits and SDMY. In Y1, r_p between SDMY and ΔRWC was −0.17 ($p = .008$).
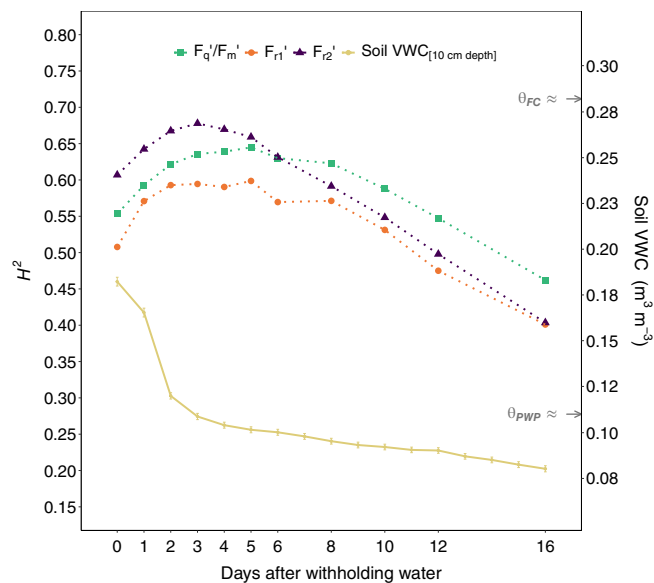
FIGURE 5 Dynamics of broad-sense heritability on an entry-mean basis (H^2) for operating efficiency of PSII (F'_q/F'_m) and both reoxidation processes, F'_{r1} and F'_{r2}, from light-adapted durum wheat plants under progressive drought stress, from 0 to 16 days after withholding water (DAWW), in Y1. The progression of soil volumetric water content (VWC) at 10 cm depth over time is also displayed. Small arrows on the right-hand side approximate to the soil permanent wilting point (θ_{PWP}) and the soil field capacity (θ_{FC}) at 10 cm depth [Colour figure can be viewed at wileyonlinelibrary.com]

FIGURE 6 Mean trait–trait genetic correlations (r_g) ± SE, $n = 252$ genotypes, from 0 to 16 days after withholding water, between each chlorophyll fluorescence trait (F'_q/F'_m, F'_{r1} and F'_{r2}) and (a) the total shoot dry matter yield (SDMY) at the end of the stress period, and (b) the relative change in leaf relative water content (ΔRWC) as a consequence of the severe drought stress imposed in Y1 [Colour figure can be viewed at wileyonlinelibrary.com]

3.7 | Environmental responses and diurnal courses of ChlF traits

Both PPFD and air VPD were major fluctuating environmental factors driving nonlinear changes in the ChlF traits from light-adapted plants within a measurement day. In fact, their interaction effect (log$PPFD \cdot$ logVPD; i.e., both variables were log-transformed) was especially important for accounting for the variations observed in the ChlF traits under severe drought, as in Y1 (Table S10). Increasing light intensity from 150 to 2,500 µmol m^{-2} s^{-1} induced a continuous but nonlinear reduction in F'_q/F'_m (Figure S13a) and a deceleration in F'_{r2} (Figure S13c). Furthermore, such effects were even more pronounced when VPD increased from 1.5 to 2.5 kPa. F'_{r1} (Figure S13b) accelerated under higher VPD, especially at low light intensity (<~450 µmol m^{-2} s^{-1}), whereas this effect was negligible when PPFD was >~900 µmol m^{-2} s^{-1}. Neither the PPFD-by-VPD interaction nor its interaction with water treatments were significant ($p > .10$) for explaining the variations in the ChlF traits in Y2. Accordingly, these effects were dropped from the final fitted models. Nevertheless, the single main effects of logPPFD and logVPD were still important in Y2 and did show similar trends as in Y1 (Table S10). Notably, solely for F'_{r1} trait (Table S10), the logVPD-by-water treatment interaction effect was significant, indicating that the faster rate of F'_{r1} induced by increasing VPD occurred even more rapidly in WD than in WW plants (Figure S13d).
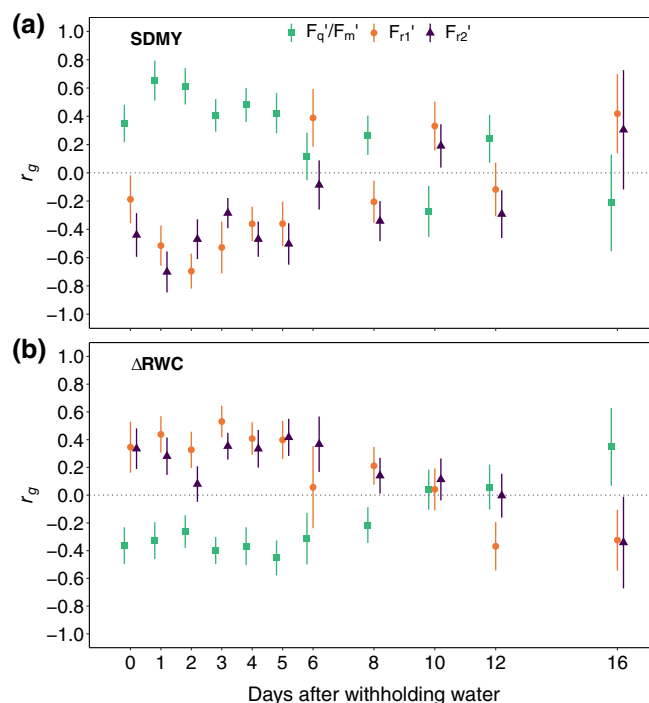
Over the course of the day, ChlF traits exhibited clear patterns which were consistent across multiple days and growing seasons, and generally followed diurnal courses of PPFD and VPD (Figures 8 and S14). The diurnal course of F'_q/F'_m (Figures 8b and S14b) showed a local minimum around midday at the peak of incoming sunlight. Relative to WW conditions (Figure 8b), WD plants tended to have slightly higher F'_q/F'_m values towards the afternoon, when PPFD was decreasing but VPD was at the highest. The diurnal course of F'_{r2} (Figures 8d and S14d) mirrored that displayed by F'_q/F'_m, showing a local maximum (i.e., slowest rate) around midday. However, there were no evident changes between diurnal patterns of WD and WW plants (Figure 8d). By contrast, F'_{r1} (Figures 8c and S14c) was stable early morning to midday and then decreased linearly (i.e., gradually accelerating the rates of Q_A^- reoxidation) towards the afternoon. Although stressed plants always had faster rates of F'_{r1} throughout the day (Figure 8c), especially in the afternoon under increasing VPD and decreasing PPFD, the shape of the diurnal patterns of WW and WD plants were comparable.

4 | DISCUSSION

Changes in LIFT-measured ChlF traits of light-adapted durum wheat plants subjected to progressive soil drying were induced in both the
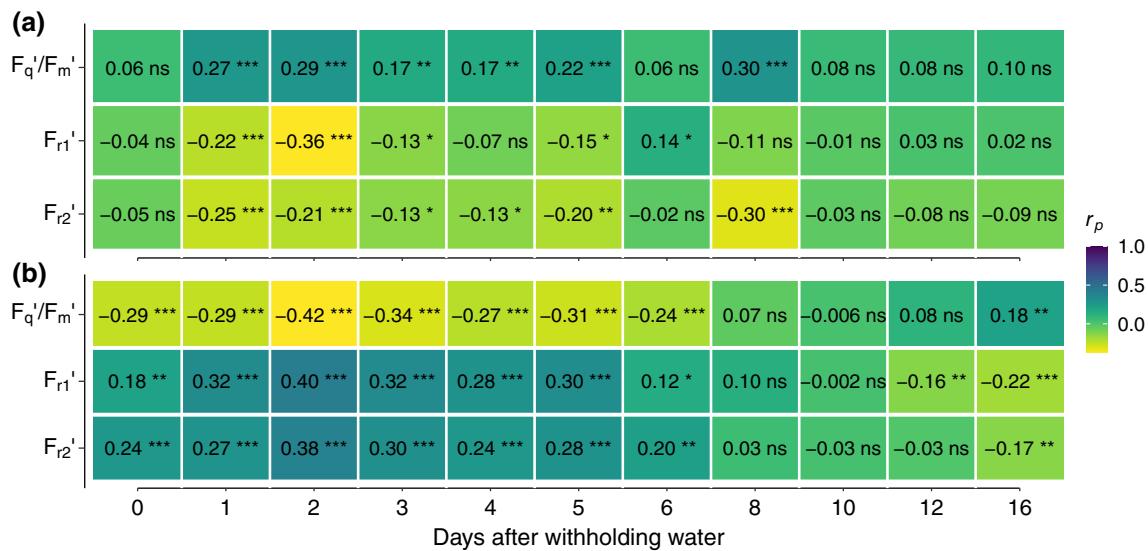
FIGURE 7 Pearson's coefficients of correlation (r_p), $n = 252$ genotypes, over time (days after withholding water) between each chlorophyll fluorescence trait (F'_q/F'_m, F'_{r1} and F'_{r2}) and (a) the total shoot dry matter yield (SDMY) at the end of the stress period, and (b) the relative change in leaf relative water content (ΔRWC) induced by the severe drought stress imposed in Y1. The levels of significance are indicated by *ns* (nonsignificant; $p > .05$), * ($p \leq .05$), ** ($p \leq .01$), and *** ($p \leq .001$) [Colour figure can be viewed at wileyonlinelibrary.com]

short and long term. In fact, a reduced photosynthetic activity, estimated by the LIFT parameters (F'_q/F'_m, F'_{r1} and F'_{r2}), was only observed under a persistent moderate to severe drought (Figure 1c). It is worthy of note, though, that the absence of a contiguous control treatment (WW) in Y1 may have limited our ability to isolate small changes caused solely by drought, particularly when it was not severe. Indeed, the photosynthetic machinery, especially PSII photochemistry, is known to be relatively resilient to water stress (Flexas et al., 2009; Flexas, Escalona, & Medrano, 1998; Havaux, 1992; Kaiser, 1987). Such a resilience, however, has been shown to be more pronounced for ChlF traits measured in dark-adapted plants as the maximum quantum efficiency of PSII photochemistry (F_v/F_m), rather than in light-adapted plants as F'_q/F'_m (Athar & Ashraf, 2005; Lu & Zhang, 1999; Zivcak et al., 2014). Therefore, these findings indicate that light-adapted ChlF traits might be physiologically preferable for assessing the effects of environmental stressors.

Concurrent electron acceptor sinks (i.e., photosynthetic carbon reduction and carbon oxidation) may explain the high resilience of ChlF traits, particularly F'_q/F'_m and F'_{r2}, even after 10 days of water-limiting conditions in Y1 (Figure 1c) and also the fact that no declines relative to WW plants were found under mild drought in Y2. Stomatal (g_s) and mesophyll (g_m) conductance are key CO_2 diffusion components that regulate leaf transpiration efficiency, playing pivotal roles in plant acclimation to drought (Flexas et al., 2009; Ouyang, Struik, Yin, & Yang, 2017). In the short term, at the onset of water-limiting conditions, stomatal closure is induced to reduce water loss and thereby CO_2 availability, leading to increased photorespiration (Cornic, 2000; Lawlor, 2002). In C_3 plants under mild drought, the O_2 uptake via photorespiratory activity can almost entirely replace the lower CO_2 availability as an electron acceptor pathway (Cornic & Fresneau, 2002). Drought-stressed tomato plants, for instance,

doubled electron dissipation through photorespiration relative to non-stressed plants (Haupt-Herting & Fock, 2002). This repartitioning of light energy, or energy balancing network (Walker, Kramer, Fisher, & Fu, 2020), may result in minor changes in ChlF-based traits in mild stress. Nevertheless, if drought progresses, LET might be electron sink-limited, as both photorespiration and the Calvin-Benson cycle can be repressed, causing impairment of ribulose bisphosphate (RuBP) regeneration and adenosine triphosphate (ATP) synthesis (Flexas & Medrano, 2002; Tezara, Mitchell, Driscoll, & Lawlor, 1999). Ultimately, whole photosynthetic electron transport activity will be down-regulated (Cornic & Fresneau, 2002; Haupt-Herting & Fock, 2002; Medrano, Escalona, Bota, Gulías, & Flexas, 2002; Schöttler & Tóth, 2014). Hence, these considerations can explain the decrease in F'_q/F'_m co-occurring with reduced F'_{r1} and F'_{r2} in response to long-term severe drought stress observed in Y1.

The very strong linear relationship between F'_q/F'_m and F'_{r2} (i.e., the kinetics of electron transport from PQ pool towards PSI; Figure 3b) supports the mechanism of photosynthetic control of electron transfer when metabolism is repressed under environmental stresses to prevent photodamage in both PSII and PSI. According to Kanazawa et al. (2017), ATP synthase activity decreases in limiting CO_2, slowing proton efflux from the thylakoid lumen and, consequently, increasing proton motive force (*pmf*) across the thylakoid membrane. As a consequence, a more acidic lumen can concomitantly (a) trigger the energy-dependent (q_E) non-photochemical quenching (NPQ), which thermally dissipates the surplus of absorbed light energy from the light-harvesting complexes (LHCs) to prevent over-excitation of PSII, as well as (b) slow down the electron transfer through the cytochrome b_6f complex (Cytb_6f), which prevents over-reduction of PSI electron acceptors (Kanazawa et al., 2017; Tikhonov, 2013). These mechanisms of photoprotection governed by ATP synthase activity
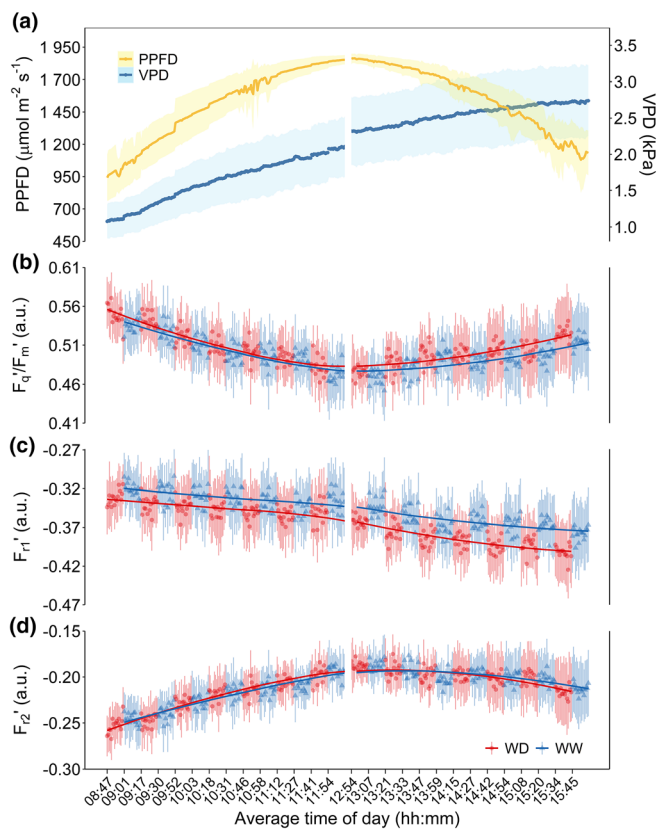
FIGURE 8 Diurnal course of (a) photosynthetic photon flux density (PPFD) and air vapour pressure deficit (VPD), (b) operating efficiency of PSII (F'_q/F'_m) and both reoxidation processes, (c) F'_{r1} and (d) F'_{r2}, for well-watered (WW) and water-limited (WD) durum wheat plants in light-adapted conditions in Y2. Values are $M \pm SD$, averaged across days of field phenotyping, $n = 9$. The local time zone is Mountain Standard Time (MST). The discontinuity around midday relates to a daily operational break during the LIFT data collection (see details in Figure S3) [Colour figure can be viewed at wileyonlinelibrary.com]

are known to be at the core of plant acclimation to long-term drought stress (Kohzuma et al., 2009). Therefore, a slower F'_{r2} might suggest a deceleration of electrons through Cytb_6f with simultaneous decreasing in F'_q/F'_m due to a higher NPQ.

Regardless of drought, LIFT-measured ChlF traits displayed similar diurnal temporal patterns (Figures 8 and S14), which demonstrate the high level of inherent regulation of the photosynthetic apparatus under fluctuating growing conditions, particularly through, but not limited to, NPQ. Similar patterns have also been observed in various other plant species growing in open fields (Pieruschka et al., 2010, 2014; Raesch et al., 2014). Instantaneous light intensity and temperature have been reported by Keller, Matsubara, et al. (2019) as the key drivers of such dynamics, in agreement with our findings. Actually, because air VPD is strongly correlated with air temperature (Figure S15; Gates, Zolnier, & Buxton, 1998; Yuan et al., 2019) and includes air relative humidity, we investigated the impacts of VPD instead. It is well known that adjustments in the PSII/PSI stoichiometry are crucial to optimize the quantum

efficiency of photosynthesis under fluctuating environment (Chow, Melis, & Anderson, 1990; Külheim, Ågren, & Jansson, 2002). Recently, Grieco et al. (2020) reported short- and long-term photosynthetic adjustments to drought and fluctuating light in wheat by changing NPQ relaxation and the PSII-LHCII phosphorylation pattern combined with a fine-tuning in protein stoichiometry. Indeed, the efficiency of electron transport under changing ambient conditions is highly dependent on the tight co-ordination among the several electron carriers between PSII and PSI, whose intricate regulatory processes occur at different time scales and multiple sites (see details in Dietz, 2015; Horton, 2012; Kono & Terashima, 2014; Rochaix, 2011; Schöttler & Tóth, 2014; Tikkanen et al., 2012; Walters, 2005).

The sustained faster F'_{r1} (i.e., the kinetics of electron transport from Q_A towards PQ pool) in Y2 relative to control (Figure 8c) was the most remarkable effect of mild drought. This suggests that plants could sense a subtle shortage of soil moisture, quickly modulate their photosynthetic electron transport and potentially trigger responses to either acclimate or cope with reduced water availability. Interestingly, increasing atmospheric VPD intensified this response (Figure S13d). We hypothesize that stomata responses combined with alternative electron flows apart from the LET, such as water–water cycle (WWC), cyclic electron flow around PSI (CEF) and/or chlororespiration mediated by the plastid terminal oxidase (PTOX) (Cruz et al., 2005; Kono & Terashima, 2014), might explain a faster F'_{r1} at the onset of drought. Takahashi, Milward, Fan, Chow, and Badger (2009) demonstrated that CEF enhances the *pmf* and helps to alleviate photoinhibition by either suppressing photodamage to PSII via a q_E-independent mechanism or preventing the inhibition of the repair of photodamaged PSII via a q_E-dependent mechanism. It has long been recognized that CEF enhances under drought (Golding, Finazzi, & Johnson, 2004; Golding & Johnson, 2003; Zivcak et al., 2014). In addition, PTOX mediates the electron transfer from plastoquinol (PQH_2) to reduce O_2 to H_2O via a non-electrogenic process (Shirao et al., 2013), potentially acting as a safety valve by protecting the PQ pool and mediating physiological responses (Krieger-Liszkay & Feilke, 2016; McDonald et al., 2011; Nawrocki, Tourasse, Taly, Rappaport, & Wollman, 2015). Indeed, both CEF and PTOX are dependent on the redox state of the PQ pool, a vital component of photosynthesis with multiple functions, including photoprotection and stress tolerance (Havaux, 2020). Remarkably, Wang et al. (2016) recently demonstrated the role of the PQ pool over-reduction as a mechanism of chloroplast-mediated stomatal closure. Moreover, it is known that rising VPD increases atmospheric demand for water, leading to stomatal closure (Franks, Cowan, & Farquhar, 1997; Massmann, Gentine, & Lin, 2019). Besides VPD, diurnal and seasonal stomata kinetics are also driven by combined effects of temperature, irradiance and soil moisture (Matthews, Vialet-Chabrand, & Lawson, 2018; McAusland et al., 2016; Neukam, Böttcher, & Kage, 2016; Sack & Holbrook, 2006). Altogether, early changes in F'_{r1} may appear as acclimation responses to the onset of water-limiting conditions, which might promote photoprotection, even when drought stress effects are not obvious at the whole-plant level.

Our results show dynamic fluctuations in broad-sense heritability for ChlF traits (Figure 5) due to changes in the relative contribution of genetic variance over time. Even after correcting the ChlF traits for biological (e.g., plant height, phenology and canopy reflectance) and environmental (e.g., PPFD and VPD) variations, strong significant differences between genotypes were still found, demonstrating that there was substantial genetic variability that could not be explained by those covariates alone. Araus, Amaro, Voltas, Nakkoul, and Nachit (1998) have similarly reported genetic variability for ChlF traits in durum wheat under field conditions, where phenology was also considered. In our data, the highest H^2 for F'_q/F'_m, F'_{r1} and F'_{r2} were observed in mild drought but with gradual reductions when the soil became drier. It is noteworthy that H^2 values estimated in Y2 (milder drought) were of similar orders of magnitude as in Y1 at the onset of drought stress (i.e., when the soil VWC of both seasons were comparable). Using a high-throughput image phenotyping approach, Chen et al. (2014) also observed dynamic changes in heritability over time for fluorescence-based traits in barley under drought, where H^2 similarly decreased during progressive stress. Time-varying H^2 for F'_q/F'_m in *Arabidopsis* growing in fluctuating light has also been reported by Flood et al. (2016). It has been argued that the dynamic change of heritability over time is due to changes in the magnitude of genotype and environment effects, as well as their interaction (Visscher, Hill, & Wray, 2008). Fluctuations in H^2 for a trait can be challenging for plant breeding programmes, particularly in drought-prone environments, where a lower heritability under severe stress could negatively impact the effectiveness of selection.

The changing genetic and phenotypic correlations between ChlF traits and above-ground biomass yield (Figures 6a and 7a) or ΔRWC (Figures 6b and 7b) during soil drying might suggest that multiple water use strategies are in place to cope with water deficit. In mild drought, genotypes with high photosynthetic activity tended to have both high biomass yield and high dehydration, altogether indicating a high transpiration rate. As the opposite behaviour was also true (i.e., low photosynthetic activity with low biomass yield and low dehydration), the identification of water savers and spenders (Nakhforoosh, Bodewein, Fiorani, & Bodner, 2016) may be somewhat facilitated by ChlF values, at least under mild stress. Nonetheless, such correlations were weaker, or even shifted directions, in severe drought. These circumstances were probably due to other traits related to drought tolerance which may also affect ChlF responses, including stay-green (delayed senescence), osmotic adjustment and antioxidant defence (Chen et al., 2017; Christopher, Christopher, Borrell, Fletcher, & Chenu, 2016; Farooq, Hussain, & Siddique, 2014). It is also known that plants under drought stress can adapt by altering biomass partitioning among roots and grain development (Davies & Zhang, 1991; Fang et al., 2017). However, it was beyond the scope of our study to evaluate root dynamics and possible changes due to drought.

Apart from the high level of phenotypic plasticity for ChlF traits among genotypes, a crossover interaction was noticed (Figure 4), especially for F'_{r1} and F'_{r2}, which reinforces the roles of genotype-by-time (i.e., drought severity) effect and the genetic complexity of plant

responses to drought. In other words, genotypes with high photosynthetic activity (high F'_q/F'_m and fast F'_{r1} and F'_{r2}) in non-limiting environments will likely perform worse when grown under very poor conditions compared to those with low photosynthetic activity, and vice versa. A crossover effect has also been reported for grain yield (Araus, Slafer, Reynolds, & Royo, 2002; Araus, Slafer, Royo, & Serret, 2008; Cooper, Stucker, DeLacy, & Harch, 1997) and is a "source of frustration" (Blum, 2005) to plant breeding for drought stress adaptation. Properly setting the target environment, therefore, seems to be essential for accurate comprehension of and good use of the genetic variation in ChlF traits.

5 | CONCLUSIONS

We here demonstrated that short- and long-term changes in ChlF traits induced by progressive drought were rapidly and non-invasively monitored at canopy level in durum wheat under field conditions. Integrating LIFT-measured ChlF traits with high temporal resolution environmental data facilitated the assessment of genotype-by-environment interaction effects under drought stress. Simultaneous statistical modelling of spatial patterns and temporal trends combined with time-varying covariates helped to improve the precision and interpretation of experiments under changing ambient conditions. Strong significant differences in ChlF traits were found among genotypes, demonstrating that there is substantial genetic variability available for breeding programmes to select for drought-adaptive traits. This also suggests that the LIFT method can enable genome-wide association studies (GWAS) for dissecting the QTLome of photosynthetic traits and assess the effects on yield associated with the relevant quantitative trait loci (QTLs). At an unprecedented scale, our high-throughput approach for field phenotyping ChlF traits not only allowed for estimation of genetic effects over time in a large durum wheat panel but also shed light on the diurnal dynamics of the photosynthetic apparatus, leveraging the ability to dissect complex physiological traits. We propose that plant ecophysiology studies and physiological plant breeding benefit from more flexible and versatile methods to measure photosynthesis and related traits, enabling knowledge of the mechanisms of drought adaption under natural plant stand and agricultural field conditions alike.

DATA AVAILABILITY STATEMENT
The data that support the findings of this study are openly available in "Zenodo" at https://doi.org/10.5281/zenodo.4305673, and in the supplementary material of this article.

ORCID
Nícolas Zendonadi dos Santos https://orcid.org/0000-0002-3365-6060

Hans-Peter Piepho https://orcid.org/0000-0001-7813-2992

Giuseppe Emanuele Condorelli https://orcid.org/0000-0002-8052-0844

Eder Licieri Groli https://orcid.org/0000-0001-9191-0058
Maria Newcomb https://orcid.org/0000-0003-2974-9149
Richard Ward https://orcid.org/0000-0003-4436-0019
Roberto Tuberosa https://orcid.org/0000-0001-9143-9569
Marco Maccaferri https://orcid.org/0000-0002-1935-3282
Fabio Fiorani https://orcid.org/0000-0001-8775-1541
Uwe Rascher https://orcid.org/0000-0002-9993-4588
Onno Muller https://orcid.org/0000-0002-0473-5632

REFERENCES
Aasen, H., van Wittenberghe, S., Medina, N. S., Damm, A., Goulas, Y., Wieneke, S., ... Mac, A. A. (2019). Sun-induced chlorophyll fluorescence II: Review of passive measurement setups, protocols, and their application at the leaf to canopy level. *Remote Sensing*, 11(8), 927.

Allen R. G., Pereira L. S., Raes D. & Smith M. (1998). *Crop Evapotranspiration: guidelines for computing crop water requirements* (FAO Irrigation and Drainage Paper No. 56). Rome, Italy: FAO.

Ananyev, G., Kolber, Z. S., Klimov, D., Falkowski, P. G., Berry, J. A., Rascher, U., ... Osmond, B. (2005). Remote sensing of heterogeneity in photosynthetic efficiency, electron transport and dissipation of excess light in *Populus deltoids* stands under ambient and elevated CO_2 concentrations, and in a tropical forest canopy, using a new laser-induced fluorescence transient device. *Global Change Biology*, 11(8), 1195–1206.

Araus, J. L., Amaro, T., Voltas, J., Nakkoul, H., & Nachit, M. M. (1998). Chlorophyll fluorescence as a selection criterion for grain yield in durum wheat under Mediterranean conditions. *Field Crops Research*, 55(3), 209–223.

Araus, J. L., & Cairns, J. E. (2014). Field high-throughput phenotyping: The new crop breeding frontier. *Trends in Plant Science*, 19(1), 52–61.

Araus, J. L., Slafer, G. A., Reynolds, M. P., & Royo, C. (2002). Plant breeding and drought in C_3 cereals: What should we breed for? *Annals of Botany*, 89(7), 925–940.

Araus, J. L., Slafer, G. A., Royo, C., & Serret, M. D. (2008). Breeding for yield potential and stress adaptation in cereals. *Critical Reviews in Plant Science*, 27(6), 377–412.

Athar, H. R., & Ashraf, M. (2005). Photosynthesis under drought stress. In M. Pessaraki (Ed.), *Handbook of photosynthesis* (2nd ed., pp. 793–809). Boca Raton, FL: CRC Press.

Baker, N. R. (2008). Chlorophyll fluorescence: A probe of photosynthesis in vivo. *Annual Review of Plant Biology*, 59(1), 89–113.

Baker, N. R., & Rosenqvist, E. (2004). Applications of chlorophyll fluorescence can improve crop production strategies: An examination of future possibilities. *Journal of Experimental Botany*, 55(403), 1607–1621.

Barbagallo, R. P., Oxborough, K., Pallett, K. E., & Baker, N. R. (2003). Rapid, noninvasive screening for perturbations of metabolism and plant growth using chlorophyll fluorescence imaging. *Plant Physiology*, 132(2), 485–493.

Barrs, H. D., & Weatherley, P. E. (1962). A re-examination of the relative turgidity technique for estimating water deficits in leaves. *Australian Journal of Biological Sciences*, 15(3), 413–428.

Blum, A. (2005). Drought resistance, water-use efficiency, and yield potential – Are they compatible, dissonant, or mutually exclusive? *Australian Journal of Agricultural Research*, 56(11), 1159–1168.

Bruning, B., Berger, B., Lewis, M., Liu, H., & Garnett, T. (2020). Approaches, applications, and future directions for hyperspectral vegetation studies: An emphasis on yield-limiting factors in wheat. *The Plant Phenome Journal*, 3(1), e20007.

Cendrero-Mateo, M. P., Moran, M. S., Papuga, S. A., Thorp, K. R., Moreno, L. A., Ponce-Campos, G., ... Wang, G. (2016). Plant chlorophyll fluorescence: Active and passive measurements at canopy and leaf scales with different nitrogen treatments. *Journal of Experimental Botany*, 67(1), 275–286.

Cendrero-Mateo, M. P., Muller, O., Albrecht, H., Burkat, A., Gatzke, S., Janssen, B., ... Rascher, U. (2017). Field phenotyping: Concepts and examples to quantify dynamic plant traits across scales in the field. In A. Chabbi & H. W. Loescher (Eds.), *Terrestrial ecosystem research infrastructures: Challenges and opportunities* (pp. 53–80). Boca Raton, FL: CRC Press.

Chen, D., Neumann, K., Friedel, S., Kilian, B., Chen, M., Altmann, T., & Klukas, C. (2014). Dissecting the phenotypic components of crop plant growth and drought responses based on high-throughput image analysis. *The Plant Cell*, 26(12), 4636–4655.

Chen, Y. E., Cui, J. M., Su, Y. Q., Zhang, C. M., Ma, J., Zhang, Z. W., ... Yuan, S. (2017). Comparison of phosphorylation and assembly of photosystem complexes and redox homeostasis in two wheat cultivars with different drought resistance. *Scientific Reports*, 7, 12718.

Cheng, J., Edwards, L. J., Maldonado-Molina, M. M., Komro, K. A., & Muller, K. E. (2010). Real longitudinal data analysis for real people: Building a good enough mixed model. *Statistics in Medicine*, 29(4), 504–520.

Chow, W. S., Melis, A., & Anderson, J. M. (1990). Adjustments of photosystem stoichiometry in chloroplasts improve the quantum efficiency of photosynthesis. *Proceedings of the National Academy of Sciences of the United States of America*, 87(19), 7502–7506.

Christopher, J. T., Christopher, M. J., Borrell, A. K., Fletcher, S., & Chenu, K. (2016). Stay-green traits to improve wheat adaptation in well-watered and water-limited environments. *Journal of Experimental Botany*, 67(17), 5159–5172.

Condorelli, G. E., Maccaferri, M., Newcomb, M., Andrade-Sanchez, P., White, J. W., French, A. N., ... Tuberosa, R. (2018). Comparative aerial and ground based high throughput phenotyping for the genetic dissection of NDVI as a proxy for drought adaptive traits in durum wheat. *Frontiers in Plant Science*, 9, 893.

Cooper, M., Stucker, R. E., DeLacy, I. H., & Harch, B. D. (1997). Wheat breeding nurseries, target environments, and indirect selection for grain yield. *Crop Sciences*, 37(4), 1168–1176.

Cornic, G. (2000). Drought stress inhibits photosynthesis by decreasing stomatal aperture – Not by affecting ATP synthesis. *Trends in Plant Science*, 5(5), 187–188.

Cornic, G., & Fresneau, C. (2002). Photosynthetic carbon reduction and carbon oxidation cycles are the main electron sinks for photosystem II activity during a mild drought. *Annals of Botany*, 89(7), 887–894.

Cruz, J. A., Avenson, T. J., Kanazawa, A., Takizawa, K., Edwards, G. E., & Kramer, D. M. (2005). Plasticity in light reactions of photosynthesis for energy production and photoprotection. *Journal of Experimental Botany*, 56(411), 395–406.

Cullis, B. R., Smith, A. B., & Coombes, N. E. (2006). On the design of early generation variety trials with correlated data. *Journal of Agricultural, Biological, and Environmental Statistics*, 11(4), 381–393.

Davies, W. J., & Zhang, J. (1991). Root signals and the regulation of growth and development of plants in drying soil. *Annual Review of Plant Physiology and Plant Molecular Biology*, 42(1), 55–76.

de Wijn, R., & van Gorkom, H. J. (2001). Kinetics of electron transfer from Q_A to Q_B in photosystem II. *Biochemistry*, 40(39), 11912–11922.

Dietz, K. J. (2015). Efficient high light acclimation involves rapid processes at multiple mechanistic levels. *Journal of Experimental Botany*, 66(9), 2401–2414.

Dong, T., Liu, J., Shang, J., Qian, B., Ma, B., Kovacs, J. M., ... Shi, Y. (2019). Assessment of red-edge vegetation indices for crop leaf area index estimation. *Remote Sensing of Environment*, 222, 133–143.

Drusch, M., Moreno, J., Del Bello, U., Franco, R., Goulas, Y., Huth, A., ... Verhoef, W. (2017). The FLuorescence EXplorer Mission–Concept–ESA's earth Explorer 8. *IEEE Transactions on Geoscience and Remote Sensing*, 55(3), 1273–1284.

Edmeades, G. O., McMaster, G. S., White, J. W., & Campos, H. (2004). Genomics and the physiologist: Bridging the gap between genes and crop response. *Field Crops Research*, 90(1), 5–18.

Fang, Y., Du, Y., Wang, J., Wu, A., Qiao, S., Xu, B., ... Chen, Y. (2017). Moderate drought stress affected root growth and grain yield in old, modern and newly released cultivars of winter wheat. *Frontiers in Plant Science*, 8, 672.

Farooq, M., Hussain, M., & Siddique, K. H. M. (2014). Drought stress in wheat during flowering and grain-filling periods. *Critical Reviews in Plant Sciences*, 33(4), 331–349.

Filella, I., & Peñuelas, J. (1994). The red edge position and shape as indicators of plant chlorophyll content, biomass and hydric status. *International Journal of Remote Sensing*, 15(7), 1459–1470.

Flexas, J., Barón, M., Bota, J., Ducruet, J. M., Gallé, A., Galmés, J., ... Medrano, H. (2009). Photosynthesis limitations during water stress acclimation and recovery in the drought-adapted *Vitis* hybrid Richter-110 (*V. berlandieri* × *V. rupestris*). *Journal of Experimental Botany*, 60(8), 2361–2377.

Flexas, J., Escalona, J. M., & Medrano, H. (1998). Down-regulation of photosynthesis by drought under field conditions in grapevine leaves. *Australian Journal of Plant Physiology*, 25(8), 893–900.

Flexas, J., & Medrano, H. (2002). Drought-inhibition of photosynthesis in C_3 plants: Stomatal and non-stomatal limitations revisited. *Annals of Botany*, 89(2), 183–189.

Flood, P. J., Kruijer, W., Schnabel, S. K., van der Schoor, R., Jalink, H., Snel, J. F. H., ... Aarts, M. G. M. (2016). Phenomics for photosynthesis, growth and reflectance in *Arabidopsis thaliana* reveals circadian and long-term fluctuations in heritability. *Plant Methods*, 12, 14.

Franks, P. J., Cowan, I. R., & Farquhar, G. D. (1997). The apparent feedforward response of stomata to air vapour pressure deficit: Information revealed by different experimental procedures with two rainforest trees. *Plant, Cell and Environment*, 20(1), 142–145.

Galwey, N. W. (2014). *Introduction to mixed modelling: Beyond regression and analysis of variance* (2nd ed.). Chichester, UK: John Wiley & Sons.

Gates, R. S., Zolnier, S., & Buxton, J. (1998). Vapor pressure deficit control strategies for plant production. *IFAC Proceedings Volumes*, 31(12), 271–276.

Genty, B., Briantais, J. M., & Baker, N. R. (1989). The relationship between the quantum yield of photosynthetic electron transport and quenching of chlorophyll fluorescence. *Biochimica et Biophysica Acta (BBA)–General Subjects*, 990(1), 87–92.

Gilmour, A. R., Thompson, R., & Cullis, B. R. (1995). Average information REML: An efficient algorithm for variance parameter estimation in linear mixed models. *Biometrics*, 51(4), 1440–1450.

Golding, A. J., Finazzi, G., & Johnson, G. N. (2004). Reduction of the thylakoid electron transport chain by stromal reductants – Evidence for activation of cyclic electron transport upon dark adaptation or under drought. *Planta*, 220, 356–363.

Golding, A. J., & Johnson, G. N. (2003). Down-regulation of linear and activation of cyclic electron transport during drought. *Planta*, 218, 107–114.

Govindjee (2004). Advances in photosynthesis and respiration. Chlorophyll a fluorescence: A signature of photosynthesis. In G. C. Papageorgiou & Govindjee (Eds.), *Chlorophyll a fluorescence: A bit of basics and history* (Vol. 19, pp. 1–42). Dordrecht, The Netherlands: Springer.

Grieco, M., Roustan, V., Dermendjiev, G., Rantala, S., Jain, A., Leonardelli, M., ... Teige, M. (2020). Adjustment of photosynthetic activity to drought and fluctuating light in wheat. *Plant, Cell and Environment*, 43(6), 1484–1500.

Habash, D. Z., Paul, M. J., Parry, M. A. J., Keys, A. J., & Lawlor, D. W. (1995). Increased capacity for photosynthesis in wheat grown at elevated CO_2: The relationship between electron transport and carbon metabolism. *Planta*, 197, 482–489.

Haupt-Herting, S., & Fock, H. P. (2002). Oxygen exchange in relation to carbon assimilation in water-stressed leaves during photosynthesis. *Annals of Botany*, 89(7), 851–859.

Havaux, M. (1992). Stress tolerance of photosystem II in vivo: Antagonistic effects of water, heat, and photoinhibition stresses. *Plant Physiology*, 100(1), 424–432.

Havaux, M. (2020). Plastoquinone in and beyond photosynthesis. *Trends in Plant Science*, 25(12), 1252–1265.

Hayter, A. J. (1986). The maximum familywise error rate of Fisher's least significant difference test. *Journal of the American Statistical Association*, 81(396), 1000–1004.

Horton, P. (2012). Optimization of light harvesting and photoprotection: Molecular mechanisms and physiological consequences. *Philosophical Transactions of the Royal Society of London. Series B, Biological Sciences*, 367(1608), 3455–3465.

Humplík, J. F., Lazár, D., Fürst, T., Husičková, A., Hýbl, M., & Spíchal, L. (2015). Automated integrative high-throughput phenotyping of plants shoots: A case study of the cold-tolerance of pea (*Pisum sativum* L.). *Plant Methods*, 11, 20.

Jansen, M., Gilmer, F., Biskup, B., Nagel, K. A., Rascher, U., Fischbach, A., ... Walter, A. (2009). Simultaneous phenotyping of leaf growth and chlorophyll fluorescence via GROWSCREEN FLUORO allows detection of stress tolerance in Arabidopsis thaliana and other rosette plants. *Functional Plant Biology*, 36(11), 902–914.

Kaiser, W. M. (1987). Effects of water deficit on photosynthetic capacity. *Physiologia Plantarum*, 71(1), 142–149.

Kalaji, H. M., Schansker, G., Brestic, M., Bussotti, F., Calatayud, A., Ferroni, L., ... Baba, W. (2017). Frequently asked questions about chlorophyll fluorescence, the sequel. *Photosynthesis Research*, 132, 13–66.

Kanazawa, A., Ostendorf, E., Kohzuma, K., Hoh, D., Strand, D. D., Sato-Cruz, M., … Kramer, D. M. (2017). Chloroplast ATP synthase modulation of the thylakoid proton motive force: Implications for photosystem I and photosystem II photoprotection. *Frontiers in Plant Science*, *8*, 719.

Kao, W. Y., & Tsai, T. T. (1998). Tropic leaf movements, photosynthetic gas exchange, leaf δ^{13} C and chlorophyll a fluorescence of three soybean species in response to water availability. *Plant, Cell and Environment*, *21*(10), 1055–1062.

Keller, B., Matsubara, S., Rascher, U., Pieruschka, R., Steier, A., Kraska, T., & Muller, O. (2019). Genotype specific photosynthesis × environment interactions captured by automated fluorescence canopy scans over two fluctuating growing seasons. *Frontiers in Plant Science*, *10*, 1482.

Keller, B., Vass, I., Matsubara, S., Paul, K., Jedmowski, C., Pieruschka, R., … Muller, O. (2019). Maximum fluorescence and electron transport kinetics determined by light-induced fluorescence transients (LIFT) for photosynthesis phenotyping. *Photosynthesis Research*, *140*, 221–233.

Kohzuma, K., Cruz, J. A., Akashi, K., Hoshiyasu, S., Munekage, Y. N., Yokota, A., & Kramer, D. M. (2009). The long-term responses of the photosynthetic proton circuit to drought. *Plant, Cell and Environment*, *32*(3), 209–219.

Kolber, Z., Klimov, D., Ananyev, G., Rascher, U., Berry, J., & Osmond, B. (2005). Measuring photosynthetic parameters at a distance: Laser induced fluorescence transient (LIFT) method for remote measurements of photosynthesis in terrestrial vegetation. *Photosynthesis Research*, *84*, 121–129.

Kolber, Z. S., Prášil, O., & Falkowski, P. G. (1998). Measurements of variable chlorophyll fluorescence using fast repetition rate techniques: Defining methodology and experimental protocols. *Biochimica et Biophysica Acta*, *1367*(1–3), 88–106.

Kono, M., & Terashima, I. (2014). Long-term and short-term responses of the photosynthetic electron transport to fluctuating light. *Journal of Photochemistry and Photobiology B: Biology*, *137*, 89–99.

Krall, J. P., & Edwards, G. E. (1990). Quantum yields of photosystem II electron transport and carbon dioxide fixation in C$_4$ plants. *Australian Journal of Plant Physiology*, *17*(5), 579–588.

Krause, G. H., & Weis, E. (1984). Chlorophyll fluorescence as a tool in plant physiology. II. Interpretation of fluorescence signals. *Photosynthesis Research*, *5*, 139–157.

Krause, G. H., & Weis, E. (1991). Chlorophyll fluorescence and photosynthesis: The basics. *Annual Review of Plant Physiology and Plant Molecular Biology*, *42*(1), 313–349.

Krieger-Liszkay, A., & Feilke, K. (2016). The dual role of the plastid terminal oxidase PTOX: Between a protective and a pro-oxidant function. *Frontiers in Plant Science*, *6*, 1147.

Külheim, C., Ågren, J., & Jansson, S. (2002). Rapid regulation of light harvesting and plant fitness in the field. *Science*, *297*(5578), 91–93.

Lawlor, D. W. (2002). Limitation to photosynthesis in water-stressed leaves: Stomata vs. metabolism and the role of ATP. *Annals of Botany*, *89*(7), 871–885.

Lazár, D. (2003). Chlorophyll a fluorescence rise induced by high light illumination of dark-adapted plant tissue studied by means of a model of photosystem II and considering photosystem II heterogeneity. *Journal of Theoretical Biology*, *220*(4), 469–503.

Lazár, D., & Jablonský, J. (2009). On the approaches applied in formulation of a kinetic model of photosystem II: Different approaches lead to different simulations of the chlorophyll a fluorescence transients. *Journal of Theoretical Biology*, *257*(2), 260–269.

le Maire, G., François, C., & Dufrêne, E. (2004). Towards universal broad leaf chlorophyll indices using PROSPECT simulated database and hyperspectral reflectance measurements. *Remote Sensing of Environment*, *89*(1), 1–28.

Littell, R. C., Pendergast, J., & Natarajan, R. (2000). Modelling covariance structure in the analysis of repeated measures data. *Statistics in Medicine*, *19*(13), 1793–1819.

Liu J., Miller J. R., Haboudane D., & Pattey E. (2004). *Exploring the relationship between red edge parameters and crop variables for precision agriculture*. 2004 IEEE international geoscience and remote sensing symposium proceedings. Science for society: Exploring and managing a changing planet. II, IEEE, Anchorage, AK. 1276–1279. https://doi.org/10.1109/IGARSS.2004.1368649

Liu, L., Wang, J., Huang, W., Zhao, C., Zhang, B., & Tong, Q. (2004). Estimating winter wheat plant water content using red edge parameters. *International Journal of Remote Sensing*, *25*(17), 3331–3342.

Longenberger, P. S., Smith, C. W., Duke, S. E., & McMichael, B. L. (2009). Evaluation of chlorophyll fluorescence as a tool for the identification of drought tolerance in upland cotton. *Euphytica*, *166*, 25–33.

Lu, C., & Zhang, J. (1999). Effects of water stress on photosystem II photochemistry and its thermostability in wheat plants. *Journal of Experimental Botany*, *50*(336), 1199–1206.

Maccaferri, M., Sanguineti, M. C., Demontis, A., El-Ahmed, A., del Moral, L. G., Maalouf, F., … Tuberosa, R. (2011). Association mapping in durum wheat grown across a broad range of water regimes. *Journal of Experimental Botany*, *62*(2), 409–438.

Maccaferri, M., Sanguineti, M. C., Natoli, V., Ortega, J. L. A., Salem, M. B., Bort, J., … Tuberosa, R. (2006). A panel of elite accessions of durum wheat (*Triticum durum* Desf.) suitable for association mapping studies. *Plant Genetic Resources*, *4*(1), 79–85.

Marquet, P. A., Quiñones, R. A., Abades, S., Labra, F., Tognelli, M., Arim, M., & Rivadeneira, M. (2005). Scaling and power-laws in ecological systems. *The Journal of Experimental Biology*, *208*, 1749–1769.

Massmann, A., Gentine, P., & Lin, C. (2019). When does vapor pressure deficit drive or reduce evapotranspiration? *Journal of Advances in Modeling Earth Systems*, *11*(10), 3305–3320.

Mathobo, R., Marais, D., & Steyn, J. M. (2017). The effect of drought stress on yield, leaf gaseous exchange and chlorophyll fluorescence of dry beans (*Phaseolus vulgaris* L.). *Agricultural Water Management*, *180*, 118–125.

Matthews, J. S. A., Vialet-Chabrand, S., & Lawson, T. (2018). Acclimation to fluctuating light impacts the rapidity of response and diurnal rhythm of stomatal conductance. *Plant Physiology*, *176*(3), 1939–1951.

Maxwell, K., & Johnson, G. N. (2000). Chlorophyll fluorescence–A practical guide. *Journal of Experimental Botany*, *51*(345), 659–668.

McAusland, L., Atkinson, J. A., Lawson, T., & Murchie, E. H. (2019). High throughput procedure utilising chlorophyll fluorescence imaging to phenotype dynamic photosynthesis and photoprotection in leaves under controlled gaseous conditions. *Plant Methods*, *15*, 109.

McAusland, L., Vialet-Chabrand, S., Davey, P., Baker, N. R., Brendel, O., & Lawson, T. (2016). Effects of kinetics of light-induced stomatal responses on photosynthesis and water-use efficiency. *New Phytologist*, *211*(4), 1209–1220.

McDonald, A. E., Ivanov, A. G., Bode, R., Maxwell, D. P., Rodermel, S. R., & Hüner, N. P. A. (2011). Flexibility in photosynthetic electron transport: The physiological role of plastoquinol terminal oxidase (PTOX). *Biochimica et Biophysica Acta (BBA)–Bioenergetics*, *1807*(8), 954–967.

Medrano, H., Escalona, J. M., Bota, J., Gulías, J., & Flexas, J. (2002). Regulation of photosynthesis of C$_3$ plants in response to progressive drought: Stomatal conductance as a reference parameter. *Annals of Botany*, *89*(7), 895–905.

Mohammed, G. H., Colombo, R., Middleton, E. M., Rascher, U., van der Tol, C., Nedbal, L., … Zarco-Tejada, P. J. (2019). Remote sensing of solar-induced chlorophyll fluorescence (SIF) in vegetation: 50 years of progress. *Remote Sensing of Environment*, *231*, 111177.

Mullan, D., & Pietragalla, J. (2012). Leaf relative water content. In A. J. D. Pask, J. Pietragalla, D. M. Mullan, & M. P. Reynolds (Eds.), *Physiological breeding II: A field guide to wheat phenotyping* (pp. 25–27). Mexico, DF: CIMMYT.

Murchie, E. H., & Lawson, T. (2013). Chlorophyll fluorescence analysis: A guide to good practice and understanding some new applications. *Journal of Experimental Botany*, *64*(13), 3983–3998.

Mutanga, O., & Skidmore, A. K. (2007). Red edge shift and biochemical content in grass canopies. *ISPRS Journal of Photogrammetry and Remote Sensing*, 62(1), 34–42.

Nakhforoosh, A., Bodewein, T., Fiorani, F., & Bodner, G. (2016). Identification of water use strategies at early growth stages in durum wheat form shoot phenotyping and physiological measurements. *Frontiers in Plant Science*, 7, 1155.

Nawrocki, W. J., Tourasse, N. J., Taly, A., Rappaport, F., & Wollman, F. A. (2015). The plastid terminal oxidase: Its elusive function points to multiple contributions to plastid physiology. *Annual Review of Plant Biology*, 66(1), 49–74.

Neukam, D., Böttcher, U., & Kage, H. (2016). Modelling wheat stomatal resistance in hourly time steps from micrometeorological variables and soil water status. *Journal of Agronomy and Crop Science*, 202(3), 174–191.

NOAA. (2020). *Climate at a glance: Divisional rankings*. (National Centers for environmental information). Retrieved July 14, 2020, from https://www.ncdc.noaa.gov/cag/divisional/rankings/0206/zndx/201804

Nogués, S., & Alegre, L. (2002). An increase in water deficit has no impact on the photosynthetic capacity of field-grown Mediterranean plants. *Functional Plant Biology*, 29(5), 621–630.

O'Neill, P. M., Shanahan, J. F., & Schepers, J. S. (2006). Use of chlorophyll fluorescence assessments to differentiate corn hybrid response to variable water conditions. *Crop Science*, 46(2), 681–687.

Osmond, B., Chow, W. S., Pogson, B. J., & Robinson, S. A. (2019). Probing functional and optical cross-sections of PSII in leaves during state transitions using fast repetition rate light induced fluorescence transients. *Functional Plant Biology*, 46(6), 567–583.

Osmond, B., Chow, W. S., Wyber, R., Zavafer, A., Keller, B., Pogson, B. J., & Robinson, S. A. (2017). Relative functional and optical absorption cross-sections of PSII and other photosynthetic parameters monitored in situ, at a distance with a time resolution of a few seconds, using a prototype light induced fluorescence transient (LIFT) device. *Functional Plant Biology*, 44(10), 985–1006.

Oukarroum, A., Madidi, S. E., Schansker, G., & Strasser, R. J. (2007). Probing the responses of barley cultivars (*Hordeum vulgare* L.) by chlorophyll a fluorescence OLKJIP under drought stress and re-watering. *Environmental and Experimental Botany*, 60(3), 438–446.

Ouyang, W., Struik, P. C., Yin, X., & Yang, J. (2017). Stomatal conductance, mesophyll conductance, and transpiration efficiency in relation to leaf anatomy in rice and wheat genotypes under drought. *Journal of Experimental Botany*, 68(18), 5191–5205.

Patterson, H. D., & Williams, E. R. (1976). A new class of resolvable incomplete block designs. *Biometrika*, 63(1), 83–92.

Payne, R., Welham, S., & Harding, S. (2019). *A guide to REML in Genstat* (20th ed.). Hemel Hempstead, Hertfordshire, UK: VSN International.

Pérez-Bueno, M. L., Pineda, M., & Barón, M. (2019). Phenotyping plant responses to biotic stress by chlorophyll fluorescence imaging. *Frontiers in Plant Science*, 10, 1135.

Piepho, H. P. (2018). Allowing for the structure of a designed experiment when estimating and testing trait correlations. *The Journal of Agricultural Science*, 156(1), 59–70.

Piepho, H. P. (2019). A coefficient of determination (R^2) for generalized linear mixed models. *Biometrical Journal*, 61(4), 860–872.

Piepho, H. P., Büchse, A., & Emrich, K. (2003). A Hitchhiker's guide to mixed models for randomized experiments. *Journal of Agronomy and Crop Science*, 189(5), 310–322.

Piepho, H. P., Büchse, A., & Richter, C. (2004). A mixed modelling approach for randomized experiments with repeated measures. *Journal of Agronomy and Crop Science*, 190(4), 230–247.

Piepho, H. P., & Möhring, J. (2011). On estimation of genotypic correlations and their standard errors by multivariate REML using the MIXED procedure of the SAS system. *Crop Science*, 51(6), 2449–2454.

Piepho, H. P., Williams, E. R., & Michel, V. (2015). Beyond Latin squares: A brief tour of row-column designs. *Agronomy Journal*, 107(6), 2263–2270.

Pieruschka, R., Albrecht, H., Muller, O., Berry, J. A., Klimov, D., Kolber, Z. S., ... Rascher, U. (2014). Daily and seasonal dynamics of remotely sensed photosynthetic efficiency in tree canopies. *Tree Physiology*, 34(7), 674–685.

Pieruschka, R., Klimov, D., Kolber, Z. S., & Berry, J. A. (2010). Monitoring of cold and light stress impact on photosynthesis by using the laser induced fluorescence transient (LIFT) approach. *Functional Plant Biology*, 37(5), 395–402.

Qiao, C. G., Basford, K. E., DeLacy, I. H., & Cooper, M. (2000). Evaluation of experimental designs and spatial analyses in wheat breeding trials. *Theoretical and Applied Genetics*, 100, 9–16.

R Core Team. (2020). *R: A language and environment for statistical computing*. R Foundation for Statistical Computing, Vienna, Austria. Retrieved from https://www.R-project.org/

Raesch, A. R., Muller, O., Pieruschka, R., & Rascher, U. (2014). Field observations with laser-induced fluorescence transient (LIFT) method in barley and sugar beet. *Agriculture*, 4(2), 159–169.

Ranalli, P., di Candilo, M., & Bagatta, M. (1997). Drought tolerance screening for potato improvement. *Plant Breeding*, 116(3), 290–292.

Rascher, U., & Pieruschka, R. (2008). Spatio-temporal variations of photosynthesis: The potential of optical remote sensing to better understand and scale light use efficiency and stresses of plant ecosystems. *Precision Agriculture*, 9, 355–366.

Reynolds, M., Chapman, S., Crespo-Herrera, L., Molero, G., Mondal, S., Pequeno, D. N. L., ... Sukumaran, S. (2020). Breeder friendly phenotyping. *Plant Science*, 295, 110396.

Robinson, G. K. (1991). That BLUP is a good thing: The estimation of random effects. *Statistical Science*, 6(1), 15–32.

Rochaix, J. D. (2011). Regulation of photosynthetic electron transport. *Biochimica et Biophysica Acta (BBA)–Bioenergetics*, 1807(3), 375–383.

Sack, L., & Holbrook, N. M. (2006). Leaf hydraulics. *Annual Review of Plant Biology*, 57(1), 361–381.

Schöttler, M. A., & Tóth, S. Z. (2014). Photosynthetic complex stoichiometry dynamics in higher plants: Environmental acclimation and photosynthetic flux control. *Frontiers in Plant Science*, 5, 188.

Schreiber, U. (1986). Detection of rapid induction kinetics with a new type of high-frequency modulated chlorophyll fluorometer. *Photosynthesis Research*, 9, 261–272.

Shirao, M., Kuroki, S., Kaneko, K., Kinjo, Y., Tsuyama, M., Förster, B., ... Badger, M. R. (2013). Gymnosperms have increased capacity for electron leakage to oxygen (Mehler and PTOX reactions) in photosynthesis compared with angiosperms. *Plant and Cell Physiology*, 54(7), 1152–1163.

Sim, C. H., Gan, F. F., & Chang, T. C. (2005). Outlier labelling with boxplot procedures. *Journal of the American Statistical Association*, 100(470), 642–652.

Stirbet, A., & Govindjee. (2011). On the relation between the Kautsky effect (chlorophyll a fluorescence induction) and photosystem II: Basics and applications of the OJIP fluorescence transient. *Journal of Photochemistry and Photobiology B: Biology*, 104(1–2), 236–257.

Stirbet, A., Lazár, D., Guo, Y., & Govindjee, G. (2020). Photosynthesis: Basics, history and modelling. *Annals of Botany*, 126(4), 511–537.

Stirbet, A. D., & Strasser, R. J. (1995). Numerical simulation of the fluorescence induction in plants. *Archives Des Sciences et Compte Rendu Des séances de la Société*, 48(1), 41–60.

Takahashi, S., Milward, S. E., Fan, D. Y., Chow, W. S., & Badger, M. R. (2009). How does cyclic electron flow alleviate photoinhibition in Arabidopsis? *Plant Physiology*, 149(3), 1560–1567.

Tezara, W., Mitchell, V. J., Driscoll, S. D., & Lawlor, D. W. (1999). Water stress inhibits plant photosynthesis by decreasing coupling factor and ATP. *Nature*, 401, 914–917.

Tikhonov, A. N. (2013). pH-dependent regulation of electron transport and ATP synthesis in chloroplasts. *Photosynthesis Research*, 116, 511–534.

Tikkanen, M., Grieco, M., Nurmi, M., Rantala, M., Suorsa, M., & Aro, E. M. (2012). Regulation of the photosynthetic apparatus under fluctuating growth light. *Philosophical transactions of the Royal Society of London. Series B, Biological Sciences*, 367, 3486–3493.

Tschiersch, H., Junker, A., Meyer, R. C., & Altmann, T. (2017). Establishment of integrated protocols for automated high throughput kinetic chlorophyll fluorescence analyses. *Plant Methods*, 13, 54.

Tuberosa, R. (2012). Phenotyping for drought tolerance of crops in the genomics era. *Frontiers in Physiology*, 3, 347.

van Eeuwijk, F. A., Bustos-Korts, D., Millet, E. J., Boer, M. P., Kruijer, W., Thompson, A., ... Chapman, S. C. (2019). Modelling strategies for assessing and increasing the effectiveness of new phenotyping techniques in plant breeding. *Plant Science*, 282, 23–39.

van Genuchten, M. T. (1980). A closed-form equation for predicting the hydraulic conductivity of unsaturated soils. *Soil Science Society of America Journal*, 44(5), 892–898.

Virlet, N., Sabermanesh, K., Sadeghi-Tehran, P., & Hawkesford, M. J. (2017). Field scanalyzer: An automated robotic field phenotyping platform for detailed crop monitoring. *Functional Plant Biology*, 44(1), 143–153.

Visscher, P. M., Hill, W. G., & Wray, N. R. (2008). Heritability in the genomics era–Concepts and misconceptions. *Nature Reviews Genetics*, 9, 255–266.

Vogelmann, J. E., Rock, B. N., & Moss, D. M. (1993). Red edge spectral measurements from sugar maple leaves. *International Journal of Remote Sensing*, 14(8), 1563–1575.

VSN International. (2019). *Genstat for windows* (20th ed.). Hemel Hempstead, UK: VSN International.

Wada, S., Takagi, D., Miyake, C., Makino, A., & Suzuki, Y. (2019). Responses of the photosynthetic electron transport reactions stimulate the oxidation of the reaction center chlorophyll of photosystem I, P700, under drought and high temperatures in rice. *International Journal of Molecular Sciences*, 20(9), 2068.

Walker, B. J., Kramer, D. M., Fisher, N., & Fu, X. (2020). Flexibility in the energy balancing network of photosynthesis enables safe operation under changing environmental conditions. *Plants*, 9(3), 301.

Walters, R. G. (2005). Towards an understanding of photosynthetic acclimation. *Journal of Experimental Botany*, 56(411), 435–447.

Wang, H., Qian, X., Zhang, L., Xu, S., Li, H., Xia, X., ... Liu, X. (2018). A method of high throughput monitoring crop physiology using chlorophyll fluorescence and multispectral imaging. *Frontiers in Plant Science*, 9, 407.

Wang, W. H., He, E. M., Chen, J., Guo, Y., Chen, J., Liu, X., & Zheng, H. L. (2016). The reduced state of the plastoquinone pool is required for chloroplast-mediated stomatal closure in response to calcium stimulation. *The Plant Journal*, 86(2), 132–144.

Wang, Z. X., Chen, L., Ai, J., Qin, H. Y., Liu, Y. X., Xu, P. L., ... Zhang, Q. T. (2012). Photosynthesis and activity of photosystem II in response to drought stress in Amur grape (*Vitis amurensis* Rupr.). *Photosynthetica*, 50(2), 189–196.

White, J. W., & Conley, M. M. (2013). A flexible, low-cost cart for proximal sensing. *Crop Science*, 53(4), 1646–1649.

Wolfinger, R. (1993). Covariance structure selection in general mixed models. *Communications in Statistics–Simulation and Computation*, 22 (4), 1079–1106.

Wyber, R., Osmond, B., Ashcroft, M. B., Malenovský, Z., & Robinson, S. A. (2018). Remote monitoring of dynamic canopy photosynthesis with high time resolution light-induced fluorescence transients. *Tree Physiology*, 38(9), 1302–1318.

Xin, C. P., Yang, J., & Zhu, X. G. (2013). A model of chlorophyll a fluorescence induction kinetics with explicit description of structural constraints of individual photosystem II units. *Photosynthesis Research*, 117, 339–354.

Yan, H., Wu, L., Filardo, F., Yang, X., Zhao, X., & Fu, D. (2017). Chemical and hydraulic signals regulate stomatal behavior and photosynthetic activity in maize during progressive drought. *Acta Physiologiae Plantarum*, 39, 125.

Yuan, W., Zheng, Y., Piao, S., Ciais, P., Lombardozzi, D., Wang, Y., ... Yang, S. (2019). Increased atmospheric vapor pressure deficit reduces global vegetation growth. *Science Advances*, 5(8), eaax1396.

Zadoks, J. C., Chang, T. T., & Konzak, C. F. (1974). A decimal code for the growth stages of cereals. *Weed Research*, 14(6), 415–421.

Zhu, X. G., Govindjee, Baker, N. R., deSturler, E., Ort, D. R., & Long, S. P. (2005). Chlorophyll a fluorescence induction kinetics in leaves predicted from a model describing each discrete step of excitation energy and electron transfer associated with photosystem II. *Planta*, 223, 114–133.

Zivcak, M., Kalaji, H. M., Shao, H. B., Olsovska, K., & Brestic, M. (2014). Photosynthetic proton and electron transport in wheat leaves under prolonged moderate drought stress. *Journal of Photochemistry and Photobiology B: Biology*, 137, 107–115.

SUPPORTING INFORMATION

Additional supporting information may be found online in the Supporting Information section at the end of this article.

APPENDIX A.

Criteria for data cleaning

In Y1, ChlF transients were assessed and discarded in accordance with the following: (a) Data points acquired with signal-to-noise ratio <40; (b) F'_q/F'_m values outside the 0–1 range; (c) the adjusted coefficient of determination (R^2_{adj}) from the log–log model at t_1 (for F'_{r1}) was <.95 for data collected between 0 and 6 DAWW, <.9025 for data collected at 8 and 10 DAWW, or <.81 for data at 12 and 16 DAWW; and (d) R^2_{adj} from the log–log model at t_2 (for F'_{r2}) was <.90 for data collected between 0 and 6 DAWW, <.85 for data collected at 8 and 10 DAWW, or <.80 for data at 12 and 16 DAWW. A high R^2_{adj} ensures that only reasonably formed ChlF transients (i.e., showing typical relaxation stages as close as possible to the schematic shown in Figure S4) are kept in the datasets. After performing the previous steps, outliers at plot level per day of measurement for each trait (ChlF and VOGREI) were detected and removed based on Tukey's boxplot method by using 1.5 times the interquartile range (IQR) (Sim, Gan, & Chang, 2005). As F'_q/F'_m, F'_{r1} and F'_{r2} are derived from the same transient, in the case of an outlier, none of the ChlF traits for that particular transient was considered for further analysis.

In Y2, ChlF transients were assessed and discarded as follows: (a) data points acquired with signal-to-noise ratio ≤100; (b) F'_q/F'_m values outside the 0–1 range; and (c) R^2_{adj} from the log–log models at t_1 (for F'_{r1}) and t_2 (for F'_{r2}) were <.95 and <.90, respectively, regardless of timing. Then, outliers for each trait (ChlF and VOGREI) were detected and removed at plot level per day of measurement in the same way as done in Y1.

APPENDIX B.

Model selection with mixed-effects modelling

In Y1, a linear mixed model (LMM) for each phenotype trait measured in a single day was defined as

$$\gamma = R : G + ROW + R \cdot ROW + R \cdot COL + \underline{R \cdot ROW \cdot COL}, \quad (B1)$$

where γ is the vector of observed phenotype, G stands for the genotypes, R the replicates, ROW the rows, COL the columns, and the underscored term ($R \cdot ROW \cdot COL$ in this case) is the residual error effect (ε) associated with the observation γ. All models were herein outlined according to the syntax described in Piepho, Büchse, and Emrich (2003), where the dot operator ($\cdot$) specifies crossed effects ($A \cdot B$), the crossing operator ($\times$) defines a full factorial model ($A \times B = A + B + A \cdot B$), and the nesting operator (/) describes that a factor B is nested within another factor A ($A/B = A + A \cdot B$). Fixed and random terms are separated by a colon (:), listing fixed effects first. Model (B1) took all factors except R as random and was used to fit SDMY and ΔRWC, with both traits natural log-transformed. In addition, one- and two-dimensional spatial models were fitted as residual, so covariance structures (Payne, Welham, & Harding, 2019; Wolfinger, 1993), such as autoregressive (AR), moving average (MA), autoregressive moving average (ARMA) or linear variance (LV), were used for modelling correlations among the neighbouring experimental units along rows and columns. For BLUEs estimation, G factor was fitted as fixed in the Model (B1).

Repeated measures were incorporated into the Model (B1) as proposed by Piepho, Büchse, and Richter (2004). Hence, the single-stage baseline model (BL), which considers the entire observed data in Y1 in one stage at the level of individual plots, was defined as

$$\gamma = R \times T : G/T + ROW/T + (R \cdot ROW)/T \\ + (R \cdot COL)/T + R \cdot ROW \cdot COL + \underline{R \cdot ROW \cdot COL \cdot T}, \quad (B2)$$

where T is time points (i.e., days after withholding water), the repeated factor. On top of the Model (B2), covariates were also included, and the full baseline model (BL_{Cov}) for Y1 was defined as

$$\gamma = R \times T + RelF + iZDS + VOGREI + PPFD \times VPD : VOGREI \cdot T \\ + G/T + ROW/T + (R \cdot ROW)/T + (R \cdot COL)/T \quad (B3) \\ + R \cdot ROW \cdot COL + \underline{R \cdot ROW \cdot COL \cdot T},$$

where $iZDS$ is the initial growth stage in the Zadoks scale measured 2 days before withholding water, VOGREI the Vogelmann red edge

index, PPFD the photosynthetic photon flux density, VPD the vapour pressure deficit and RelF is the relative deviation of the target area from the focal point of the LIFT light beam set at 0.60 m, calculated as $\left[\frac{LIFT_{height} - PH}{60}\right]$, where $LIFT_{height}$ is the distance from the soil surface to the LIFT lens [cm] and PH is the plant height [cm]. RelF and $iZDS$ were time-constant covariates, whilst VOGREI, PPFD and VPD were time-varying covariates. Model (B3) was used to fit F'_q/F'_m, F'_{r1} and F'_{r2}. Besides the spatial modelling of trends along rows and columns, temporal correlation structures (Littell, Pendergast, & Natarajan, 2000; Payne et al., 2019), such as compound symmetry (CS), banded Toeplitz (BAND), power (POW), ante-dependence (ANTE), unstructured (UN) or general correlation (COR), with equal or unequal variances were also fitted to the residuals to accommodate trends over time due to multiple observations on the same experimental unit. Modelling of serial correlation was also extended to $G \cdot T$ in order to assess genetic correlations for the same trait across time, allowing for heterogeneity of genetic variances. For estimating BLUEs for each time point, G/T were fitted as fixed in the Model (B3).

In Y2, a LMM for each phenotype trait measured in each time point after imposing water treatment was defined as

$$\gamma = TRT + R : G/TRT + ROW/SUB + R \cdot ROW + R \cdot COL \\ + R \cdot ROW \cdot COL + R \cdot ROW \cdot SUB + \underline{R \cdot COL \cdot ROW \cdot SUB}, \quad (B4)$$

where TRT is the water treatment and SUB the subrows. Model (B4) was used to fit SDMY, which was natural log-transformed. For estimating BLUEs within each water treatment, G/TRT were fitted as fixed in the model (B4).

For assessing the differences among levels of drought severity, repeated measures were incorporated into the Model (B4). Therefore, the BL model, which considers the entire observed data in Y2 in one stage at the level of individual plots, was defined as

$$\gamma = (TRT + R) \times T : G/T + (G \cdot TRT)/T + ROW/T + (ROW \cdot SUB)/T \\ + (R \cdot ROW)/T + (R \cdot COL)/T + (R \cdot ROW \cdot COL)/T \\ + (R \cdot ROW \cdot SUB)/T + R \cdot COL \cdot ROW \cdot SUB \\ + \underline{R \cdot COL \cdot ROW \cdot SUB \cdot T}, \quad (B5)$$

where T is time points after imposing water treatment (i.e., the levels of drought severity), the repeated factor. Covariates were also added as fixed in the Model (B5) to account for the fluctuating environment, and so the BL_{Cov} model for Y2 was defined as

$$\gamma = (TRT + R + RelF + ZDS + VOGREI) \times T \\ + (RelF + ZDS + VOGREI + PPFD \times VPD) \times TRT : G/T + (G \cdot TRT)/T \\ + ROW/T + (ROW \cdot SUB)/T + (R \cdot ROW)/T + (R \cdot COL)/T \\ + (R \cdot ROW \cdot COL)/T + (R \cdot ROW \cdot SUB)/T + R \cdot COL \cdot ROW \cdot SUB \\ + \underline{R \cdot COL \cdot ROW \cdot SUB \cdot T}, \quad (B6)$$

where ZDS is the growth stage in the Zadoks scale. RelF, ZDS, VOGREI, PPFD and VPD were time-varying covariates. Model (B6) was used to fit F'_q/F'_m, F'_{r1} and F'_{r2} in Y2. Modelling of spatiotemporal

(STM) correlations was also performed for the residuals only. For estimating BLUEs within each water treatment and across time points, G/T and $(G \cdot TRT)/T$ were fitted as fixed in the Model (B6).

In all models, covariates were mean centred, except RelF which was centred to one (i.e., target area at a distance of 0.60 m). PPFD and VPD were also log-transformed and fitted to BL_{Cov} models to evaluate whether a nonlinear relationship with the ChlF traits would improve model fit.

Comparison between candidate models was assessed by the REML-likelihood ratio test (REMLRT), provided that the two models being compared were nested and had the same fixed effects model (Galwey, 2014). Otherwise, when models were non-nested, yet with the same fixed effects, the Akaike Information Criterion (AIC) was used to assess their goodness-of-fit, judged by the "smaller the better" form of the criterion (Cheng, Edwards, Maldonado-Molina, Komro, & Muller, 2010).

Bivariate LMM for estimating trait–trait genetic correlations

Assuming $\gamma = \begin{bmatrix} \gamma_1 \\ \gamma_2 \end{bmatrix}$ as the response vector of observed phenotype for the trait k ($k = 1, 2$), the bivariate model for a single time point was defined as

$$
\begin{aligned}
\gamma = {}& TRAIT + R \cdot TRAIT : G \cdot TRAIT + ROW \cdot TRAIT + R \cdot ROW \cdot TRAIT \\
& + R \cdot COL \cdot TRAIT + \underline{R \cdot ROW \cdot COL \cdot TRAIT},
\end{aligned}
$$

$$\text{(B7)}$$

where TRAIT stands for the traits of interest. Model (B7) was used to assess the correlation between SDMY and ΔRWC in Y1. Covariates were also accommodated to the bivariate models for assessing the genetic correlations between each ChlF trait and SDMY or ΔRWC in Y1 as

$$
\begin{aligned}
\gamma = {}& Z \cdot RelF + Z \cdot iZDS + Z \cdot VOGREI + Z \cdot (PPFD \times VPD) \\
& + TRAIT + R \cdot TRAIT : G \cdot TRAIT + ROW \cdot TRAIT + R \cdot ROW \cdot TRAIT \\
& + R \cdot COL \cdot TRAIT + \underline{R \cdot ROW \cdot COL \cdot TRAIT},
\end{aligned}
$$

$$\text{(B8)}$$

where is a quantitative Z variable, being set to $Z = 0$ when TRAIT = SDMY or ΔRWC, and to $Z = 1$ when TRAIT $= F'_q/F'_m$, F'_{r1} or F'_{r2}.

Coefficients of genotypic correlation between pairs of traits were defined as

$$
\rho_g = \frac{\sigma_{g_1 g_2}}{\sqrt{\sigma^2_{g_1} \times \sigma^2_{g_2}}},
$$

where $\sigma_{g_1 g_2}$ is the genetic covariance between two traits, $\sigma^2_{g_1}$ and $\sigma^2_{g_2}$ are the genotypic variances of both traits under analysis; such variance–covariance components were estimated through the random $G \cdot TRAIT$ effect in the Models (B7) or (B8). The REML estimate of ρ_g is denoted as r_g. The REMLRT was used to estimate the significance of the genetic correlations by comparing the model with varying genetic covariance between the two traits and the model with the genetic covariance fixed to zero.